



Building the First Galaxies—Chapter 2. Starbursts Dominate the Star Formation Histories of $6 < z < 12$ Galaxies

Alan Dressler¹ , Marcia Rieke² , Daniel Eisenstein³ , Daniel P. Stark² , Chris Burns¹ , Rachana Bhatawdekar^{4,5} ,
Nina Bonaventura^{2,6,7} , Kristan Boyett^{8,9} , Andrew J. Bunker¹⁰ , Stefano Carniani¹¹ , Stephane Charlot¹² ,
Ryan Hausen¹³ , Karl Misselt², Sandro Tacchella^{14,15} , and Christopher Willmer²

¹ The Observatories, The Carnegie Institution for Science, 813 Santa Barbara Street, Pasadena, CA 91101, USA; dressler@carnegiescience.edu

² Steward Observatory, University of Arizona, 933 North Cherry Avenue, Tucson, AZ 85721, USA

³ Center for Astrophysics | Harvard & Smithsonian, 60 Garden Street, Cambridge, MA 02138, USA

⁴ European Space Agency (ESA), ⁵ European Space Astronomy Centre (ESAC), Camino Bajo del Castillo s/n, E-28692 Villanueva de la Cañada, Madrid, Spain

⁶ European Space Agency, ESA/ESTEC, Keplerlaan 1, 2201 AZ Noordwijk, The Netherlands

⁷ Cosmic Dawn Center (DAWN), Copenhagen, Denmark

⁸ Niels Bohr Institute, University of Copenhagen, Jagtvej 128, DK-2200, Copenhagen, Denmark

⁹ School of Physics, University of Melbourne, Parkville 3010, VIC, Australia

¹⁰ ARC Centre of Excellence for All Sky Astrophysics in 3 Dimensions (ASTRO 3D), Australia

¹¹ Department of Physics, University of Oxford, Denys Wilkinson Building, Keble Road, Oxford OX1 3RH, UK

¹² Scuola Normale Superiore, Piazza dei Cavalieri 7, I-56126 Pisa, Italy

¹³ Sorbonne Université, CNRS, UMR 7095, Institut d’Astrophysique de Paris, 98 bis bd Arago, F-75014 Paris, France

¹⁴ Department of Physics and Astronomy, The Johns Hopkins University, 3400 North Charles Street, Baltimore, MD 21218, USA

¹⁵ Cavendish Laboratory, University of Cambridge, 19 JJ Thomson Avenue, Cambridge, CB3 0HE, UK

¹⁶ Kavli Institute for Cosmology, University of Cambridge, Madingley Road, Cambridge, CB3 0HA, UK

Received 2023 June 7; revised 2023 November 7; accepted 2023 November 21; published 2024 March 27

Abstract

We use *SEDz**—a code designed to chart the star formation histories (SFHs) of $6 < z < 12$ galaxies—to analyze the spectral energy distributions (SEDs) of 894 galaxies with deep JWST/NIRCam imaging by JADES in the GOODS-S field. We show how *SEDz** matches observed SEDs using stellar-population templates, graphing the contribution of each epoch by epoch to confirm the robustness of the technique. Very good SED fits for most SFHs demonstrate the compatibility of the templates with stars in the first galaxies—as expected, because their light is primarily from main-sequence A stars, free of post-main-sequence complexity, and insensitive to heavy-element compositions. We confirm earlier results from Dressler et al. (1) There are four types of SFHs: SFH1, burst; SFH2, stochastic; SFH3, “contiguous” (three epochs), and SFH4, “continuous” (four to six epochs). (2) Starbursts—both single and multiple—are predominant ($\sim 70\%$) in this critical period of cosmic history, although longer SFHs (0.5–1.0 Gyr) contribute one-third of the accumulated stellar mass. These 894 SFHs contribute $10^{11.14}$, $10^{11.09}$, $10^{11.00}$, and $10^{10.60} M_{\odot}$ for SFH1–4, respectively, adding up to $\sim 4 \times 10^{11} M_{\odot}$ by $z = 6$ for this field. We suggest that the absence of rising SFHs could be explained as an intense dust-enshrouded phase of star formation lasting tens of Myr that preceded each of the SFHs we measure. We find no strong dependencies of SFH type with the large-scale environment; however, the discovery of a compact group of 30 galaxies, 11 of which had first star formation at $z = 11$ –12, suggests that long SFHs could dominate in rare, dense environments.

Unified Astronomy Thesaurus concepts: [Early universe \(435\)](#)

Supporting material: animation

1. Star Formation Histories and the Birth of Galaxies: JWST’s “Prime Mission”

The HST and Beyond Committee (Dressler et al. 1996) chose a prime mission for the space telescope that would become the extraordinary JWST. The unanticipated reach of the “reborn” Hubble Space Telescope (HST) to galaxies with redshifts $z = 2$ –3—only 2 billion yr after “the beginning”—held extraordinary promise for learning how the modern Universe actually began, when the first generations of stars collected into the first galaxies. Identifying this as the key moment in our origins—rather than, for example, the Big Bang—hinges on the idea that the miracle of this Universe and, more to the point, of life, is its incredible complexity. The chemical

variety and abundance that made this possible could never have built to a critical level without multiple generations of heavy element-producing stars residing in these giant reservoirs we know as galaxies.

“The Hubble,” as we now affectionately call it, took us to the trailhead of one of humanity’s greatest journeys: traveling to this remote past to follow the story of our origins back to the present day.

Central to that mission is the simple notion that galaxies began in very different conditions—“cosmic environments”—at a time when dark matter was sculpting a terrain of mountains and valleys in a formerly smooth-as-glass Universe. There and then, “ordinary matter”—the baryons that we would be made of—were gathered and concentrated by gravity in a way that would fundamentally alter the very nature of the Universe. We had asked questions: how fast, how turbulent, how explosive, how dynamic were the forces that shaped these galaxies, so different from our times, when a slow and irreversible decline

dooms this Universe to a grinding conclusion that we—fortunately—will never see.

The tremendous effort and challenge of building JWST is behind us. The unearthly, spectacular views we now have of the Universe—near and far—let us start that remarkable journey with a large, representative sample of faint, newborn galaxies, for a first look at how they survived their tumultuous births.

Where to start? A long-standing and popular approach to the study of galaxy formation and development has been to push to higher and higher redshift to compare the properties of ever-younger galaxies. JWST has already exceeded expectations with images and confirming spectroscopy of star-forming galaxies at $z \sim 13$ (Curtis-Lake et al. 2023; Robertson et al. 2023), a scant 300 Myr after the Big Bang. Other studies identify candidates for even earlier galaxies; deeper searches and microlensing by rich clusters (Treu et al. 2022) promise to provide candidates as early as redshift $z \sim 18$. However, by their very nature, such searches find extraordinary objects—the brightest sources at the earliest epochs. In order to assemble a representative sample of the first galaxies, a later starting point is required; early JWST results suggested $z \sim 12$ as an epoch where dozens of galaxies could be identified in the JWST Advanced Deep Extragalactic Survey (JADES) GOODS-S field, with numbers increasing rapidly into the many hundreds for $z \sim 6$. This motivated the choice of $6 < z < 12$ for the present study of the star formation histories (SFHs). But for their number, these are the ancestors of the common galaxies we find today.

The paper is organized as follows. Section 2 briefly reviews the methodology—the program $SEDz^*$ —the details of which can also be found in Dressler et al. (2023, hereafter Paper I). Section 3 lays the foundation for this study, showing and explaining a new format for $SEDz^*$ results, with new data that highlight the four types of SFHs. Section 4 explains how a robust, representative sample of ~ 900 galaxies was chosen from a catalog of GOODS-S sources with nine-band NIRCcam fluxes (spectral energy distributions, SEDs) from JADES. Section 5 shows 72 examples of SFHs for four redshift ranges $6 < z < 12$, as measured by $SEDz^*$. Section 6 looks for changes in the mix of SFHs over time, and Section 7 presents a summary of the birth of stellar mass—when, where, and how much—from $z \sim 12$ down to $z \sim 6$. Section 8 investigates correlations of SFHs with environment, and Section 9 looks ahead to the implications of this study for future observational and theoretical programs. Appendix A shows histograms of SFH type with local density and nearest-neighbor distance, Appendix B shows examples of SFH templates used by $SEDz^*$, and Appendix C discusses the impact of emission lines on the continuum-dominated SEDs of this study.

A standard cosmology with $\Omega_m = 0.3$, $\Omega_\Lambda = 0.7$, and $H_0 = 70 \text{ km s}^{-1} \text{ Mpc}^{-1}$ is adopted throughout.

2. A Special Tool for a Special Time

The buildup of stellar mass in a galaxy is expressed as its SFH, that is, the rate of star formation changing with time. Measuring the SFHs of galaxies has proven more than challenging, because while groups of young, massive stars are easy to recognize, populations of stars older than a billion years—though still young compared to the Universe—age in

such a way that it is not possible to tell a population of old stars from another that is even older.

As part of a galaxy survey of 6 billion yr of cosmic history, Kelson et al. (2014) developed a tool for analyzing a galaxy’s SED—basically, its rainbow of color. By measuring SEDs for galaxies observed ~ 4 Gyr earlier in cosmic history, Kelson’s analysis leveraged those observations to look back ~ 2 Gyr further, to a time when the Universe was only around half its present age.¹⁶ Because of that, the part of a galaxy’s history that could be reliably measured was extended to when the Universe had half its present age, in this way revealing a substantial fraction of a galaxy’s growth history. Applying this approach to a sample of galaxies observed at redshift $z \sim 0.4\text{--}0.8$, Dressler et al. (2018) discovered that $\sim 20\%$ of the galaxies were still growing rapidly, with increasing star formation rates (SFRs), in an era that was thought to be a time of decline for all galaxies as massive as the Milky Way.

The motivation for this study, then, emerged directly from that one. The ability to see only 1 billion yr (or at most 2) of SFH, a small part of a mature galaxy’s lifetime, stretches to “longer than the age of the Universe” during the period when JWST’s prime mission kicks in. Our job has been to gather sufficiently good SEDs, using JWST’s near-infrared camera, NIRCcam, to make accurate measurements of galaxy brightness at a series of colors—infrared light from $1\text{--}5 \mu\text{m}$. Such data can fully constrain the ages of populations of stars that make up a galaxy, and lining up their stellar masses—epoch by epoch—constitutes an SFH of how the galaxy was built.

In this paper, we show the results of our second attempt (see Paper I) to transform the flux measurements of each galaxy—its SED—into SFHs, the buildup of stellar mass over the first billion years. Our subjects are a greatly expanded sample of 894 galaxies at redshifts $6 < z < 12$ with nine-band near-infrared fluxes from JWST/NIRCcam. We provide a short description of a program code— $SEDz^*$ —written expressly for the purpose of reconstructing the histories of galaxies from the rich information encoded in their SEDs. By choosing a sample of galaxies with ages less than a billion years, their fast-evolving stellar populations will be recorded for us to play back.

The development of $SEDz^*$ followed Kelson’s maximum-likelihood Python code for analyzing galaxy SEDs from the Carnegie–Spitzer–IMACS Survey (Kelson et al. 2016) through the combination of stellar population templates. The program effectively isolated light from younger ($\lesssim 1$ Gyr) populations of main-sequence A stars and led to the discovery of “late bloomers”—the $\gtrsim 20\%$ of galaxies at $z \sim 0.5$ that produced at least 50% of their stellar mass in the previous 1 Gyr, that is, rising SFRs instead of the falling SFRs that are conventionally described as predominant after $z = 1$. These late bloomers challenge theoretical models that tightly couple the growth of galaxies to that of their dark matter halos, because while it is possible to think of mechanisms that could delay star formation, it is not easy to imagine why some halos might form so much later than all the rest.

With this approach, the program $SEDz^*$ was developed to exclusively measure SFHs of the first galaxies. In Paper I, we described the challenges associated with measuring SFHs for stellar populations with ages of the more than 1 Gyr, a deficiency turned on its head when the the population under study has an

¹⁶ An epoch we can see by “looking back in cosmic time”—thanks to the late arrival of light in transit for billions of years.

age of $\tau \lesssim 1$ Gyr. SED_z^* takes advantage of this unique astrophysical opportunity that comes from the billion-year lifetimes of A stars (Dressler & Gunn 1983; Couch & Sharples 1987). Because they evolve rapidly over a Gyr, it is possible to derive SFHs from SEDs for A star-dominated populations, and vice versa. A stars are among the simplest main-sequence stars (Morgan & Keenan 1973), basically blackbody radiators with a relatively simple internal structure and an opacity produced by hydrogen absorption and thus free from the complications of chemical abundance and post-main-sequence evolution. These are critical and unique advantages for measuring SFHs during the first billion years.

The data input to SED_z^* are SEDs—flux measurements in NIRCam’s seven wide bands.¹⁷ SED_z^* uses a nonnegative least-squares (NNLS) engine (Lawson & Hanson 1995) and custom star formation templates (Robertson et al. 2010)¹⁸ that are essentially a set of vectors that have a significant amount of “orthornormality,” as can be seen in the plots in Appendix B, where a more complete discussion of templates can be found.

For this study, SED_z^* divides redshifts $6 < z < 12$ into seven integer steps, 12, 11...6, lasting 42, 50, 61, 79, 101, 134, and 186 Myr, respectively. SED_z^* operates with two sets of SED templates, one with 10 Myr bursts (unresolved after subsequent star formation) and another characterized by constant star formation (CSF). The program builds up an SED by adding stellar population templates (starting at $z = 12$ and working down) as needed to improve the fit and evolving them forward—adding up subsequent populations to improve the fit, as measured by χ^2 . The epoch of observation (OE) is chosen as the lowest χ^2 , and the SFH is read off as the stellar mass contributed by each scaled template that, in combination, make the best fit. This can include the addition of a CSF template that signals CSF at OE. SED_z^* can combine a CSF template with a final burst template to expand its fitting possibilities, as shown in Appendix B.

SED_z^* requires no “priors” in the important sense that every trial solution, as lower-redshift templates are added one by one, is fully independent of previous ones. This allows for modeling free of any particular functional form (e.g., nonparametric) and allowing for a range of galaxy histories. However, that range is bounded; only 33 templates are used (28 bursts, $z = 12$ to $z = 6$, evolving, and 5 CSF, $z = 10, 9, 8, 7, 6$ —at the OE). Since flux ratios are fixed for each template, choosing a template constrains all seven bands. There is no fitting of individual bands, so an acceptable solution is not guaranteed; finding one also indicates that the SED can be well described by the templates.¹⁹

Paper I describes the working of the code in considerable detail, so we do not repeat it here. Also discussed in Paper I are tests of SED_z^* , including its ability to reproduce the SEDs of synthesized galaxies in a simulated deep field, from the NIRCam “Data Challenge” (Williams+2018). The Appendix of Paper I shows how test SFHs generated by combining the stellar population templates were recovered by SED_z^* , and how the distinction between bursts and extended SFHs is robust.

¹⁷ F090W, F115W, F150W, F200W, F277W, F356W, and F444W. Fluxes in the narrower bands F335M and F410M are not used in the SED fit but are valuable in showing the presence of strong emission, particularly [O III] and H α , at these redshifts.

¹⁸ The templates are based on Bruzual & Charlot (2003) models but include emission and nonstellar continuum from star-forming regions in calculating the fluxes.

¹⁹ Since the templates come from present-epoch stellar populations, suitability to very high redshift stellar populations was unknown.

As in Paper I, we neglect the potential impact of dust. We note, as before, that galaxies in our sample seem to be well described by SEDs with little or no dust, consistent with the results of several papers showing that these initial JWST-selected samples are uniformly blue (Nanayakkara et al. 2023) and fairly dust-free. Our library of stellar population templates includes sets with extinctions of $A_V = 0.4$ and 1.0. We show in Appendix Figure 13 that extinction at the level of $A_V = 0.4$ is ruled out; in fact, even $A_V = 0.1$ would produce a reddened SED not found in the 894-galaxy sample. While we did find 27 other examples of steeply rising SEDs in the current work, their identification as galaxies at high redshift is not possible with SED_z^* because of its reliance on the A-star model.²⁰ We conclude from this that our sample is by construction a “no-extinction” sample, and that it does describe more than 95% of galaxies found by deep NIRCam imaging in this field.

However, we do speculate here that the absence of rising SFHs in this and our previous study could indicate that this phase of galaxy building is largely hidden by dust, and that the SFHs we find began with 10–20 Myr of intense, dust-enshrouded star formation, then cleared by its explosive feedback.

3. Deriving SFHs of the First Galaxies with SED_z^*

In Paper I, we introduced and explained the SED_z^* code and applied it to data from the GLASS JWST/ERO program (Treu et al. 2022) from parallel imaging with NIRCam of NIRISS grism spectroscopy of the cluster Abell 2744 (Merlin et al. 2022). Some challenges in processing and calibrating one of the first deep-imaging programs—a crucial rationale for the ERO program—limited the targets of Paper I to only 24 galaxies that were judged suitable for a first measurement of SFHs.

To that point, SED_z^* had only been tested on simulated data of the NIRCam deep-imaging program (the Data Challenge; (Williams et al. 2018) and on simulated SFHs produced using SED_z^* itself, an admittedly easier test to pass. Valid questions had been raised about how different the SEDs of the earliest galaxies might be from their descendants, particularly because the nature of stellar populations at these early times was largely unknown. However, the application of SED_z^* to the first such data produced encouraging, and surprising, results, in the sense that the program was able to reproduce 24 complex nine-band SEDs with the code’s limited library of stellar population templates.²¹ In other words, SFHs with recognizable characteristics, bursts—single and multiple, with contiguous “triples,” and continuous “long SFHs,” with reasonable masses in the range of 10^8 – $10^9 M_\odot$ —fit all 24 SEDs within the errors of the photometry. Considering the limited number of stellar population templates available to SED_z^* and their unique shapes, obtaining good fits from the “get-go” was surprising and remarkable.

With the comparatively exquisite photometry from NIRCam imaging of GOODS-S for JADES in late 2022, deeper imaging data have led to an ~ 900 -galaxy sample at redshifts $6 < z < 12$, and our analysis of these new data confirms the basic conclusions of Paper I: good reproduction of observed SEDs

²⁰ If SED_z^* was applied with the highly reddened A stars of the dusty templates shown in Appendix Figure 13, the variation caused by unknown amounts of dust would overwhelm the variation that could be attributed to different ages of stars.

²¹ In fact, our first attempt to apply SED_z^* to an early photometric catalog, which expressed fluxes in μ Jy instead of the expected nanoJy, produced only the SED equivalent of gibberish.

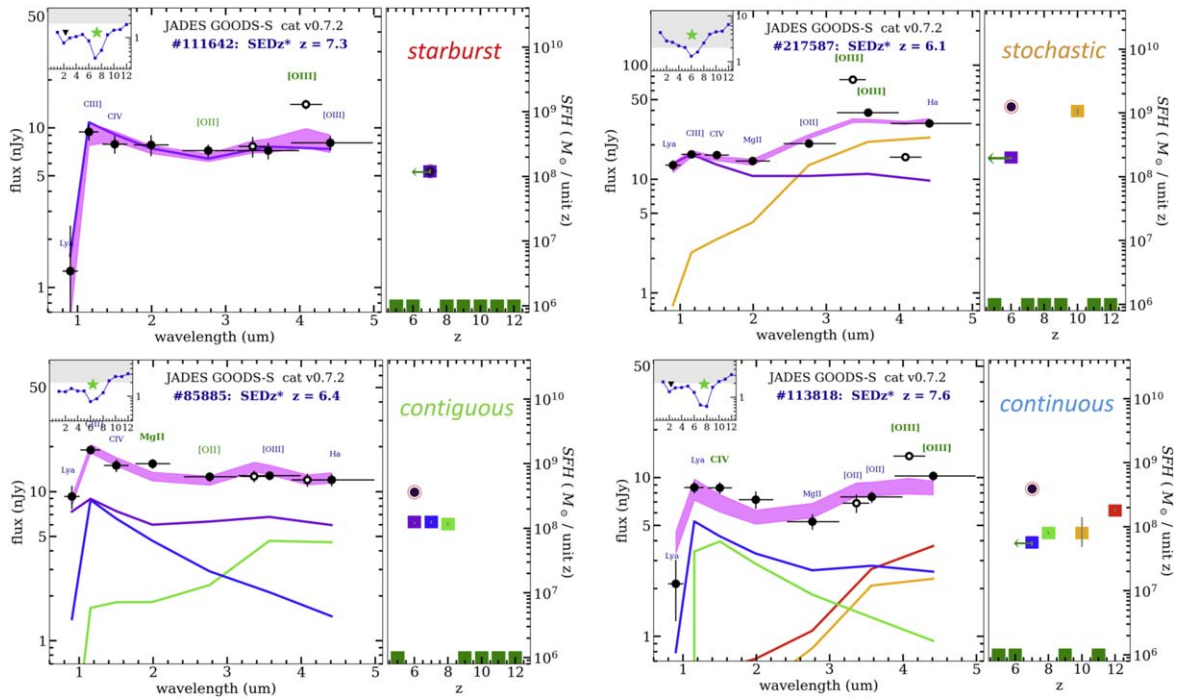


Figure 1. Examples of the four types of SFHs $6 < z < 12$ found with $SEDz^*$. The text describes how, considered together, these examples demonstrate the fidelity of $SEDz^*$ -derived SFHs. For each of the four panels, the left box shows the observed SED (black points with error bars) from nine-band NIRC*am* imaging and the NNLS fit of $SEDz^*$ (the magenta band) showing the “quartile range” of 21 trials, with all data points perturbed by 1σ random errors. The run of χ^2 is shown in the inset at upper left; the dip (green star) marks the observed redshift. Most important is the SFH corresponding to this best fit, shown in the right box. Each epoch records the stellar mass from that epoch’s star formation as a small colored box. For each epoch that contributes to the SED fit, the flux contributed to the solution is plotted in the left box as a line of the same color (below the observed SED). Error bars, based on the quartile ranges of the $SEDz^*$ fit, are typically smaller than the boxes, but a prominent exception is the $z = 10$ burst in the lower right SFH, whose contribution to the mass is uncertain within a factor of ~ 5 and may or may not contribute significantly. Error bars do not include systematic errors, such as errors associated with photometry at these faint levels, but these are unlikely to perturb the shape of the $SEDz^*$ solution. While error bars corresponding to factors of 2 uncertainty in mass are common in the large sample of the present work, such errors are not large enough to admit distinctly different SFHs. The four panels show a starburst (SFH1, upper left) and a double burst (SFH2, upper right), a “short” but contiguous run of star formation (SFH3, lower left), and a longer, continuous SFH (SFH4, lower right) covering half of the first ~ 800 Myr of cosmic history to that point. The expected locations of prominent emission lines are shown above the SED in blue; with a larger green font marks a possible detection as excess flux compared the best fit to the flux of continuum *with* emission lines. An animation of this figure is available, showing how $SEDz^*$ arrives at the best-fit SED, starting with a $z = 12$ template and adding lower-redshift templates until the minimum χ^2 is reached (as described in Section 2). Each animation starts at $z = 12$ and ends at the OE. The real-time duration of the animation is 7 s.

(An animation of this figure is available.)

and four SFH “types” and, in particular, well establishing the unexpected prominence of starburst SFHs over longer, steadier runs of star formation. Moreover, we now have sufficient data to begin to examine the dependence of these SFHs with redshift, mass, environment, and large-scale structure.

We begin by revisiting the variation in SFH type. Figure 1 introduces a new data format for $SEDz^*$ output and gives examples of the four types of SFHs found in Paper 1 and now in this paper, demonstrating both how the code derives SFHs and that it does so with considerable fidelity. The left-hand box displays the observed SED—fluxes in each of the nine bands with 1σ error bars. The NNLS solution $SEDz^*$ found by combining stellar population templates is the magenta band—the quartile range of 21 iterations, each a random perturbation of the SED by its errors. The χ^2 of the fit is inset in the upper left; a prominent minimum in χ^2 defines the observed redshift, or OE. The solution and operation of $SEDz^*$ are recorded in the right box, which shows the stellar mass added at each of seven epochs (integer redshifts $z = 12, 11 \dots 6$). This is how the SFH is calculated, by scaling and combining stellar population templates to make the best NNLS fit to the observed SED. The four plots of Figure 1 show this procedure through animation; by “clicking” on a plot, the steps $SEDz^*$ takes to derive the best-fit SFH are displayed in sequence.

In Figure 1, this “best fit” for the upper left SED is a starburst, a single epoch of star formation observed at $z = 7$ —in this case, a combination of a burst and CSF. As shown in the top-left panel of Figure 13 (Appendix B), the slope of CSF alone is more level and a burst alone much steeper than what is observed. $SEDz^*$ has determined that a ratio of 2:1 (more CSF than burst) is an excellent fit to the observed SED. That is, this two-component stellar population model from present-epoch stars in our Galaxy “works.” While it might seem remarkable that present-epoch stellar populations provide an almost perfect fit, in one sense this is completely unremarkable: the A stars that dominate the light of this starburst at the OE are the least-complicated stars along the main sequence, a fully convective core and a fully radiative envelope with opacity from hydrogen ions—no metals required.

The stellar mass calculated for star formation at $z = 7$ is $\sim 3 \times 10^8 M_{\odot}$. The green arrow signifies the CSF contribution, with ongoing star formation at OE.²² The CSF template accounts for emission at OE, detected as the modest elevation of F356W and F444W from the stellar continuum level

²² A small arrow indicates that less than half of the light comes from the CSF template (no arrow == none), and a larger arrow means more than half and as much as all.

(F410M) due to [O III] emission. The CSF template only serves at OE, because stars formed in a prior epoch are, by definition, old. In fact, although a burst or CSF is the way $SEDz^*$ models the growth of stellar mass through the epochs, these are indistinguishable by the next epoch, becoming an “old” population, regardless of how the mass was spread over the interval. It is also important to remember that, despite representing continuing CSF at OE, most of the light from the CSF template is from young A stars; the O and B stars, and any nonstellar continuum and emission are gone, except for the last 10–20 Myr.

This starburst example begs the question, could another SFH—for example, a combination of bursts—also reproduce the upper left SED? The upper right panel shows that the answer is “no” by means of an SED that is perfectly fit with a combination of two bursts: one of $\sim 5 \times 10^8 M_\odot$ at $z \approx 12$ and an $\sim 2 \times 10^8 M_\odot$ CSF+burst ~ 500 Myr later (OE $z \approx 6$). The integrated mass of this SFH is the red-encircled black dot at $\sim 7 \times 10^8 M_\odot$. Epochs without star formation are marked as lower limits of $10^6 M_\odot$. In this study, at the depth of the JADES data for the GOODS-S field, detections as low as $10^7 M_\odot$ have been made but are incomplete below $\sim 5 \times 10^7 M_\odot$ (limited by the “noise” from other epochs of star formation), and severely so below $2 \times 10^7 M_\odot$. Nevertheless, it is clear that multiple epochs of star formation cannot combine to produce the SED on the left, nor can a single epoch of star formation imitate a double.

Perhaps the most revealing feature of this double-burst example is how clearly it shows $SEDz^*$ combining two widely separated epochs of star formation to match the observed SED. The two colored curves below the SED are A-star templates that correspond to the age of the two bursts. The $z = 12$ burst in orange is that of an “old” stellar population (~ 500 Myr before OE), while the purple curve has the strong ultraviolet flux of a young population (~ 100 Myr), demonstrating the ability of $SEDz^*$ to resolve the $6 < z < 12$ epoch into old and young populations. This time it is the burst at $z = 6$ that dominates CSF, by 2:1, which accounts for the steeper slope of the purple template, as shown in the right plot in Figure 13 (Appendix B). It is the striking differences between the two templates that together reproduce the observed SED that shows how accurately $SEDz^*$ can decompose an SED into separate stellar populations, and how well an SFH can be matched with a comparatively small number of A-star templates.²³

Before moving on to examples of longer SFHs, we want to clarify why these two examples are called “starbursts,” given that each represents a few hundred million M_\odot in approximately 100 Myr. An averaged SFR of only a few $M_\odot \text{ yr}^{-1}$ is not usually considered a “burst.” However, we have no information on the history of star formation (SFR) over these individual epochs; we are not measuring SFRs but rather the total stellar mass associated with that epoch. What makes the upper left example a “burst” is that the $z = 7$ epoch contains only young A stars; that is the template that fits the SED. No older A stars—stars born in previous epochs—are detected. As we discuss in Section 9, we think it more likely that the stellar mass we find within a single epoch was born in ~ 10 – 20 Myr

early within the epoch, with SFRs in the “tens” $M_\odot \text{ yr}^{-1}$, and a falling SFR (or even a shutdown) in the 50–100 Myr after. Such “more-likely” SFHs would account for the A star-dominated SED and a corresponding absence of older A stars, $\tau \gtrsim 150$ Myr. And that is a “burst,” by any definition.

The triple-epoch SFH shown in the lower left panel is common in the sample, particularly at $z \sim 6$ – 8 . This example is particularly revealing because of the flat (purple) SFH at $z = 6$ from a CSF template that also produces [O III] and $H\alpha$ emission, a burst that contributes the peak flux at $\lambda \sim 1 \mu\text{m}$, and an ~ 200 Myr old aging burst from the $z \sim 8$ (green) burst template (but indistinguishable as a burst after $z = 8$) that produces the rising flux beyond $\sim 3 \mu\text{m}$. In addition to “contiguous,” the three epochs of star formation are close in mass at $2 \times 10^8 M_\odot$, a near-constant level of SFH that might continue to $z = 5$ and beyond. We note that a small but significant fraction of these “triples” could be fit with only two contiguous epochs of star formation, but none of them can be fit by a single epoch of SFH. And, at the redshift most are seen, two or three epochs amount to 300–400 Myr in duration, long enough to host multiple generations of star formation.

This leads naturally into the example in the lower right, where four epochs of the possible six have substantial star formation that is both continuous and, like the triple SFH, a coherent decline in added stellar mass. The most important thing to recognize about these SFHs is that, again, they cannot be reproduced by the single or a pair of bursts of star formation like in the upper left and right or by the shorter contiguous episodes that are shown in the lower left panel (see also Appendices B and C of Paper I). A long continuous SFH is defined here as four epochs or more of star formation (1) with less than a factor of 2 uncertainty in stellar mass and (2) free of two-epoch gaps. The example shown here, and the more that follow in Figures 2–5, are representative of 8% of our $6 < z < 10$ sample. It is important to reiterate that what matters for these longer, continuous SFHs is that they exist, rather than a dissection into gaps, spikes, dips, and wiggles. The data for this study are insufficient for $SEDz^*$ to deliver such detail, and indeed, this might not even be possible with higher-resolution photometric filters or spectra due to limitations in NNLS fitting. For example, a single-epoch gap in one of the continuous histories is likely a consequence of nonnegative solutions only: at any given redshift, adding star formation at that epoch may not improve the SED fit and might even degrade it. For this reason, the longer SFHs we find here are indicative of the general, not the detailed, behavior of star formation in the galaxy.

The SEDs and solutions shown Figure 1 are exemplary; they display the very good fits of a majority of SEDs to single-epoch templates (bursts) and the ability of combination templates to fit a range of SED shapes. That the fraction of cases that fail to find a good solution is small is, we think, strong evidence that the principle behind $SEDz^*$ is valid: A star-dominated stellar populations can be used to recover accurate SFHs for galaxies in the $\tau < 1$ Gyr period of cosmic history.

In the examples to follow, we will see that SFHs of significant duration are all found to be declining or nearly flat. What is almost absent from the SFHs shown here is a stretch of rising star formation. As we explained in Paper I, it is possible to attribute this to the difficulty of detecting a declining but “current” older population against a young one that was rising in flux but is now fading—a simple selection effect. However,

²³ As in the single-burst case, this double burst shows signs of star formation (elevation of the medium bands) that is contributed by CSF at $z \sim 6$. As we discuss briefly in Section 5 and show in detail in Appendix C, this emission is not responsible for the rise in red flux that is provided by star formation at $z = 12$. That contribution has already been accounted for in predicting the two broadband fluxes, F356W and F444W.

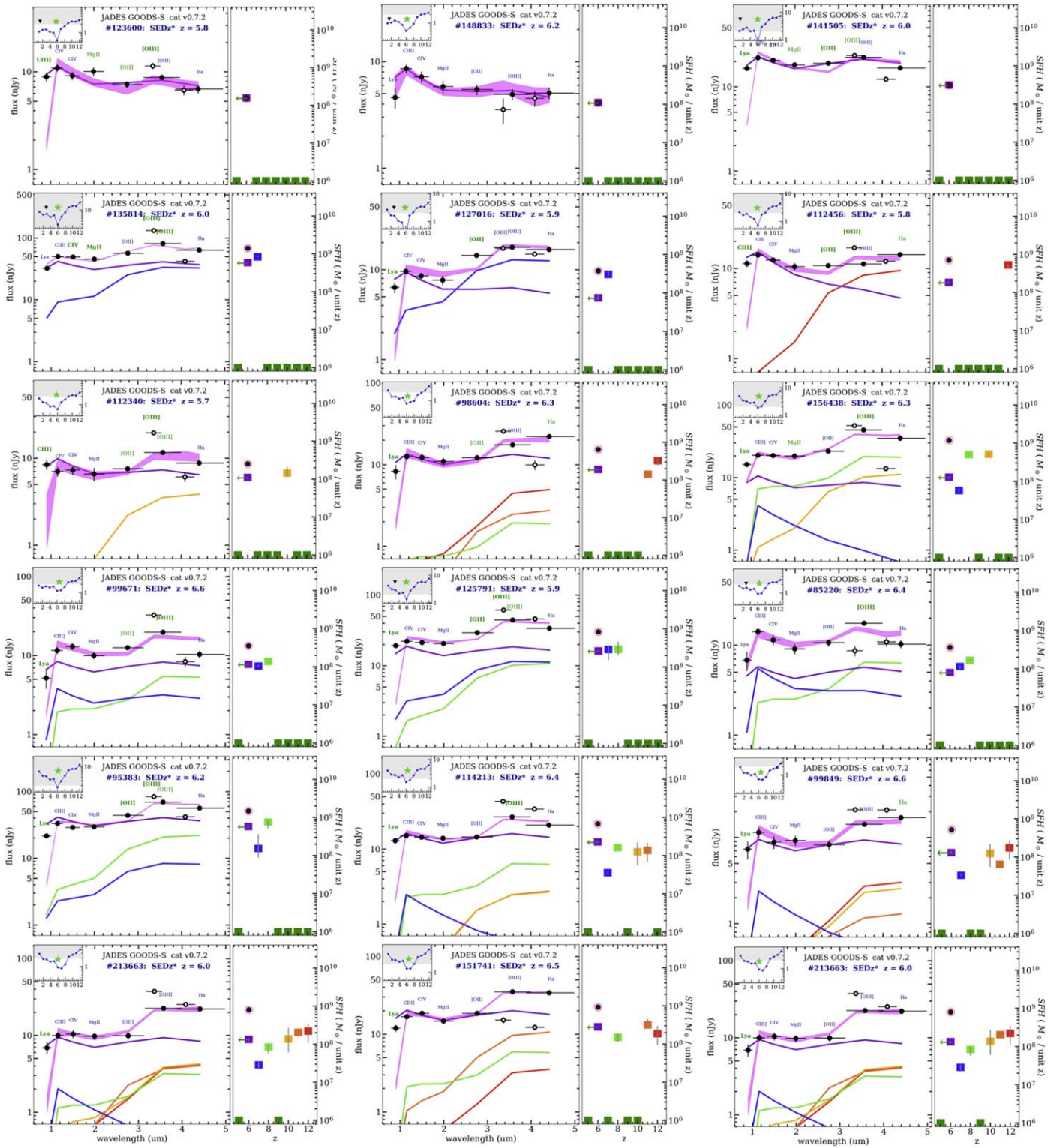


Figure 2. Examples of the four identified types of SFHs of this study observed at redshifts $z \sim 6$ ($5.75 < z < 6.75$), starting with three examples of single starbursts in the top row; continuing in order, across the rows and down, to multiburst “stochastic” histories and three-epoch contiguous runs; and finishing with long SFHs of four epochs or more. Detailed explanations of the salient characteristics of these types are given in the text.

a more intriguing possibility is that the flat/declining phases of nearly all first-galaxy SFHs—from bursts to long SFHs—were preceded by a strong, rapid burst of dusty star formation lasting $\lesssim 50$ Myr. Among the galaxies that were excluded from our sample we find 27 with steep, red SEDs, but $SEDz^*$ cannot be used to determine their redshifts, so their connection to the unobscured galaxies in our sample remains unknown.

4. Choosing a Sample of $6 < z < 12$ Galaxies

NIRCam’s exceptional performance and diversity of modes (Rieke et al. 2023) have supported Guaranteed Time Observations that cover a wide variety of science programs, including exoplanets, star formation, and our Galaxy with its neighbors. However, the largest component is devoted to the

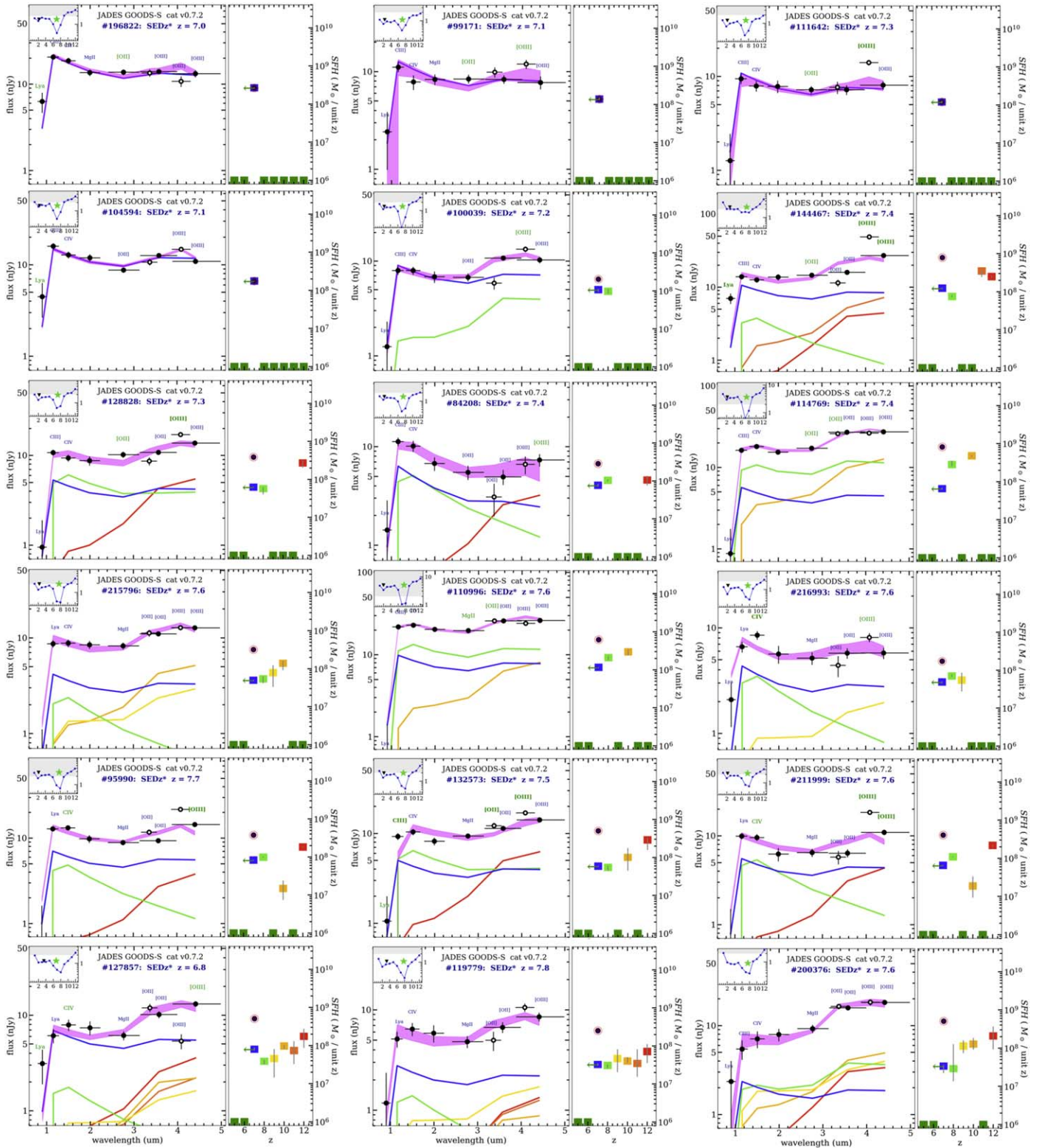


Figure 3. A virtual “replay” of the types in Figure 3 for 18 galaxies at $z \sim 7$ ($6.76 < z < 7.75$), as described in the text. This set includes five examples with very high S/N (Row(1-5);position(left-right-center) = 11, 2l, 2r, 3r, and 4c) that are exquisitely fit by $SEDz^*$ with its “present-epoch” templates, demonstrating the fidelity of the SFHs that $SEDz^*$ can deliver.

study of the early Universe (Eisenstein et al. 2023)—the era of galaxy birth. The program described in this paper comes from deep-field imaging that is beginning to answer long-standing questions about how the first generation of stars—collected into galaxies that served as reservoirs for the buildup of heavy

chemical elements—fundamentally changed the evolution of our Universe.

This study uses nine-band NIRCcam imaging of an ~ 25 arcmin² field of the JADES GOODS-S survey. The images have been intensively processed for calibration and to

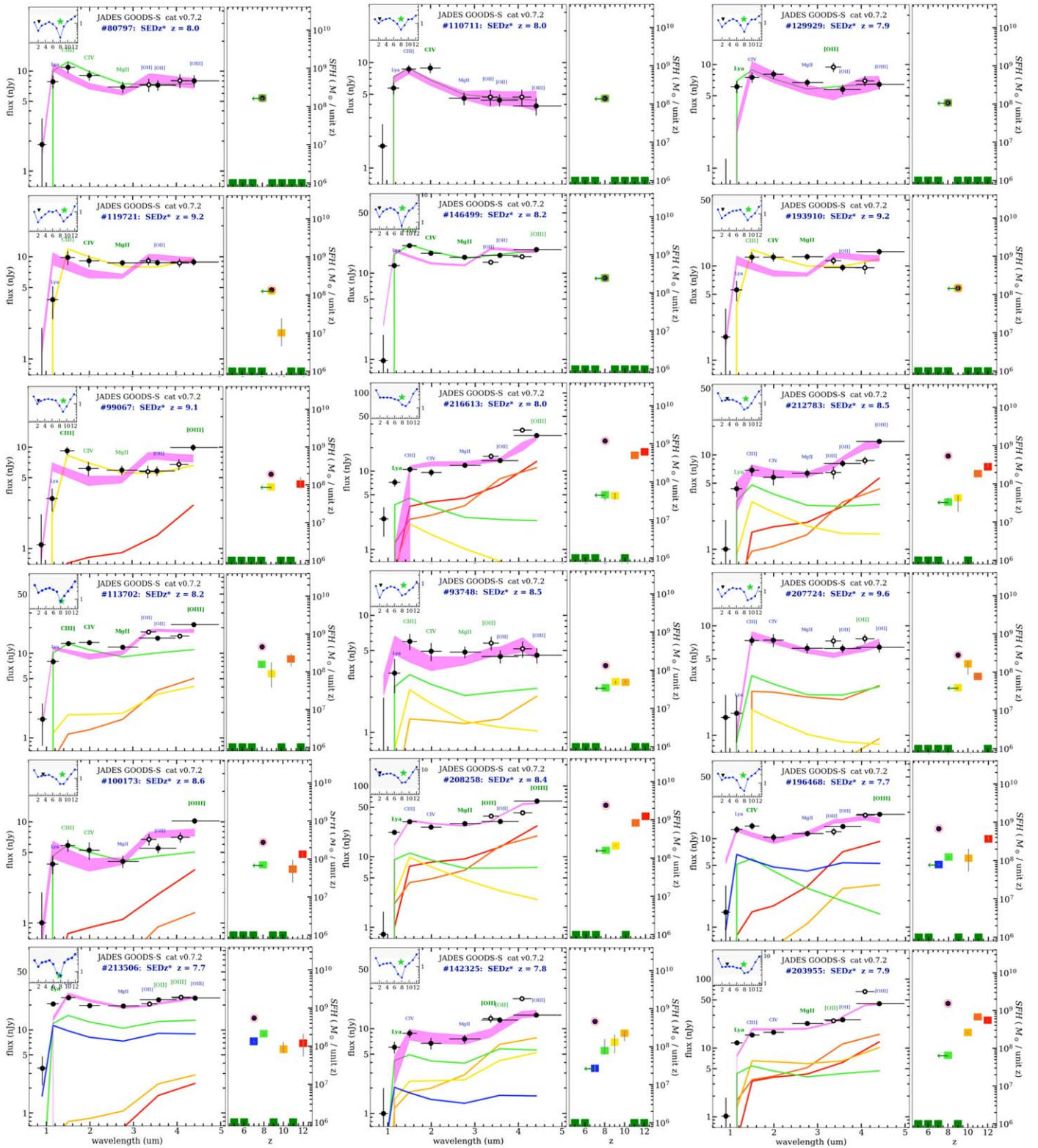


Figure 4. The persistence of the four SFH types reaches back ~ 700 Myr from $z \sim 6$. No obvious evolution of the mix of types is apparent, although changes in “proportions” may be appearing (see Figure 6). At this earlier epoch, the prominence of the Lyman break is a strong factor in finding the redshift and establishing the SFH. More than half of these $8 < z < 10$ galaxies show detected star formation back to $z \sim 11$ –12.

remove instrument signatures, combine dithered exposures, and characterize noise. These data were used to produce catalogs of objects (here v0.7.2) that identify stars and galaxies, deblend overlapping images, and generate a number of different radial extractions of photometric measurements in nine filters,

NIRCam bands F090W, F115W, F150W, F200W, F277W, F335M, F356W, F410M, and F444W. The catalog used here reached a depth of ~ 30.0 AB mag and contained 24,350 extended sources. Our study selected galaxies with a signal-to-noise ratio (S/N) $> 5\sigma$ (F200W and F277W flux) within a

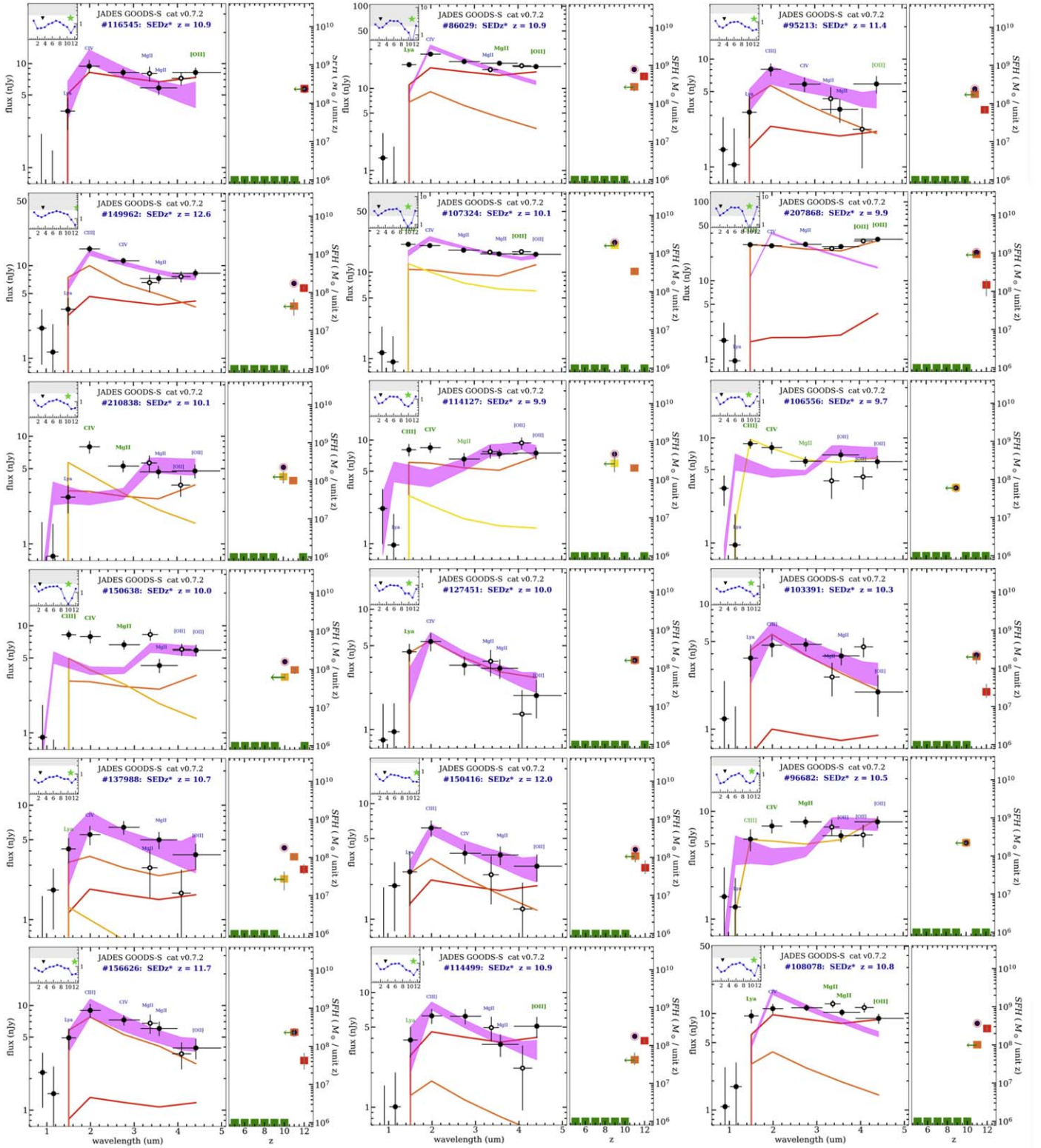


Figure 5. Eighteen of the 25 examples $z \sim 10\text{--}12$ in our 894-galaxy sample. The Lyman break now extends from F090W into the F115W filter as well. The timescale covered in this figure is only ~ 200 Myr, shorter than most of the longer histories we find at lower redshift, but there are three cases—2c, 3c, and 5l—that seem to cover this whole period.

4 pixel diameter circular aperture, appropriate for the small size of $z > 5$ galaxies. Details of data quality, data reduction, and the production of photometric catalogs can be found in Tacchella et al. (2023) and Rieke et al. (2023). To establish our sample, $SEDz^*$ was run on the complete GOODS-S v0.7.2

catalog, with results sorted into four different redshift ranges: $6 < z < 7$, $7 < z < 8$, $8 < z < 10$, and $10 < z < 13$. To be precise, the actual ranges were shifted down by 0.25 in z , for example, $5.75 < z < 6.75$, in order to center on the epoch redshift (to match the templates), in this case, $z = 6$. From the

comparison of $SEDz^*$ redshifts with the “known redshifts” of the synthetic Data Challenge, $SEDz^*$ was found to have an accuracy of $\Delta\sigma_z \approx 0.15$ for $z > 6$ galaxies. This better-than-expected performance meant that interpolation between the templates used by $SEDz^*$ was justified, and in fact, not interpolating could add to systematic errors. For this reason, boundaries were set as follows: $z1: 5.75 < z < 6.75$, $z2: 6.75 < z < 7.75$, $z3: 7.75 < z < 9.75$, and $z4: 9.75 < z < 12.75$. Thus, when a galaxy’s redshift was found to be within the range $5.75 < z < 6.25$, the $z = 6$ template was used, but when $6.25 < z < 6.75$, a 50/50 interpolation between the $z = 6$ and 7 templates was made (and so on for the other samples). In effect, this is equivalent to saying the χ^2 for $z = 6$ and 7 are the same (within errors), so the program averages the SED solutions (resulting SFHs) for those two redshifts.²⁴ Eventually, data for the separate redshift ranges would be combined into a catalog spanning the full $5.75 < z < 12.75$ range, but the previous step allowed an investigation of performance over the redshift range that was helpful.

By fitting combinations of stellar population templates, $SEDz^*$ found maximum-likelihood fits to SEDs that yielded redshifts in these four redshift intervals. A well-recognized problem in deriving $z > 4$ redshifts from SEDs is a degeneracy with $z \sim 2$ galaxies, where NIRCam’s range of $1\text{--}5\ \mu\text{m}$ translates into a rest-frame coverage of $\sim 0.3\text{--}1.7\ \mu\text{m}$, typically covering a Balmer break over an otherwise flat SED. When very faint galaxies are the targets, these are easily mistaken for $z \sim 6\text{--}8$ galaxies with a Lyman break. We used three different methods to mitigate the problem. First, we wrote code in $SEDz^*$ that compared the shape of the χ^2 curve when two minima were found, one for $z \sim 2$ and another for the higher redshift. During the Data Challenge tests, we found that using the overall slope of the run of χ^2 with redshift, the depth and width of the minima, and the color of the $SEDz^*$ itself, removed roughly 50% of cases. We also used archived HST data to find at least two 2.5σ detections in three visible bands of the WFC3 imaging, F606W, F775W, and F814W. Flux below the Lyman break is the best rejection method, but we have found that, for galaxies this faint in the near-infrared, only about one-third of low-redshift galaxies are detected in these bands, even with the deepest HST imaging available. The third check was to use EAZY “photo- z ” redshifts for the cataloged objects, part of the JADES team data processing for internal and eventual community use (Hainline et al. 2020).

The procedure was to run $SEDz^*$ for each redshift interval using only (1) the rejection of low- z objects by detection of visible flux and (2) the internal $SEDz^*$ $z < 4$ rejection. This produced the four subsets $z1$, $z2$, $z3$, and $z4$ with 759, 374, 277, and 61 galaxies, respectively. Taking the $SEDz^*$ redshift (hereafter z_{SED}) as the adopted redshift was required, because that is the value for which the SFH is derived, but comparing z_{SED} with the EAZY-derived redshift, z_a , and finding them consistent was taken as the next level of “qualification.” This was termed the “gold sample” and amounted to 446, 183, 115, and 15 “confirmed” objects. This left 313, 191, 162, and 46 objects with z_{SED} unconfirmed by z_a . Their SEDs were inspected, one by one, to decide if the Lyman-break range

was sufficiently well defined to suggest a low redshift for the galaxy. If so, the seven wideband images (readily accessed through a “*FitsMap*” viewer from the JADES image-processing team), in particular, the F090W, F115W, and F150W images, were inspected in order to evaluate visual evidence for a Lyman break. From these ~ 712 inspections, 225, 123, 103, and 38 galaxies were rejected. The remaining 88, 68, 59, and 8 galaxies were added to the “gold sample” based on judgment that at least half of these were at the higher redshift found by $SEDz^*$. The count for the four redshift slices was then $z1\text{—}534$, $z2\text{—}251$, $z3\text{—}174$, and $z4\text{—}23$, a total of 982 galaxies.

Subsequent to the first release of this paper, we “pruned” the data sample further. An additional 72 galaxies were deleted from $z1$, 18 were deleted from $z2$ and 2 were moved from $z2$ to $z3$. About half had been removed after inspection for proximity to diffraction spikes, and the remaining half was split between marginal “ $S/N \approx 5$ ” cases and poor overall fits of the model to the data. The final numbers in this study, $z1\text{—}462$, $z2\text{—}233$, $z3\text{—}176$, and $z4\text{—}23$ (unchanged)—a total of 894 galaxies.

5. Further Examples of SFHs

To expand on the introduction of the four SFH types we showed in Figure 1, we show 18 examples for each of four redshift ranges in Figures 2–5. In each, there is a row-by-row progression, starting from the top, from a single-burst population, through stochastic (multiple bursts), to contiguous epochs of star formation, and finally longer, continuous over four or more epochs.

$SEDz^*$ plots like the ones that follow, and their associated data, will be available for the full 894-galaxy sample at <https://obs.carnegiescience.edu/SEDz-star/SFHs>.

Beginning with Figure 2, we see three examples of a $z = 6$ starburst, each with a mass of $\sim 2 \times 10^8 M_\odot$. As in the discussion for the burst SFH in Figure 1, a single epoch of star formation—both occurring and observed at $z \sim 6$ —is a very good fit to each observed SED.²⁵ For all three, the solution is a combination of a burst and continuing CSF with less than a 50% contribution to the flux (denoted by the small green arrow). (A confirmation of the redshift found by $SEDz^*$ is the [O III] emission in the top left case, detected in the medium-band filter F335M.) Again, the excellent fit found for such cases validates that the stellar population templates are correct for the task. Single bursts are the most common SFHs in our study—473 cases, 53% of the full sample.

We also identify the next two examples (second row, left and center, hereafter 2l and 2c) as single bursts. Their two adjacent epochs of star formation may be unresolved, that is, one event that is best fit by using consecutive templates. In both 2l and 2c, the burst at $z = 7$ would have been very blue, but one epoch later—when these galaxies are observed—their contribution rises to the red, causing the elevation in each spectra. It seems reasonable that the star formation episode of $\tau \sim 100$ Myr could produce this $SEDz^*$ result in the relatively long “integer-redshift” epochs of $z = 6$ and 7. Under this interpretation of a single event, we include later examples where the two masses differ by as much as an order of magnitude, implying a sharply rising or falling episode of star formation.

²⁴ In some cases, averaging the two solutions appears to have stretched out the SFH by one epoch, but we could not distinguish cases where this was the right thing to do, as opposed to shifting one or the other solution. This is likely to have produced some SFH3 types from two-epoch SFH1 types. This potential, and we believe uncorrectable, error does not alter the outcome or conclusions of our study.

²⁵ Recall that the magenta band shows the quartile ranges of solutions, while the single purple line shows a single solution that is used to break down the SED into its component parts, epoch by epoch.

The next examples, which exhibit well-separated bursts, are additional demonstrations of the ability of SED_z^* to reveal dominant early star formation in galaxies observed ~ 500 Myr later, giving confidence in its identification of SFHs that extend over the $6 < z < 12$ range of our study. Comparing the stellar population templates shown in Appendix B, it is clear that these three examples show histories that cannot be reproduced by any single stellar population. Figure 2 shows three examples (2r, 3l, and 3c) of strong, well-separated bursts of star formation. We call these “stochastic” SFHs because it seems unlikely that these separate bursts can be “tied together,” not even if there was weaker, undetected star formation in between (which would be at least an order of magnitude smaller in mass). The following SFH (3r) is interpreted as either three or four epochs of star formation starting at $z = 10$. All four are graphic illustrations of very young, blue stellar populations whose red flux has been “boosted” by older populations at $z = 10\text{--}12$. For all four of these stochastic SFHs, redshifts are again confirmed by [O III] emission in the F335M band. Stochastic star formation, by our definition, is almost as common as the single bursts (in total epochs of star formation), adding 165 cases (19%) of two or more bursts. Together, “bursts” and “stochastic” make up 72% of the SFHs found here; clearly, this is a strong and, we believe, unexpected dominant mode of galaxy building in its beginnings.

However, the bottom three rows of Figure 2 remind us that a significant fraction of early galaxies are undergoing more orderly, gradual growth. In examples 4l, 4c, 4r, and 5l, three stellar populations are required to fit the observed SEDs. SFH3 star formation is usually “contiguous” but sometimes with a one-epoch gap, likely due to “noise” or the asymmetry in NNLS solutions—no negative star formation. (See Figure 3, the gap in 4c, but note the $z = 9$ star formation 4l that shows the opposite—a detection that is dubious.) SFH3 describes 21% of the full sample (25% of the $z = 6$ sample). All three have final star formation at $z = 6$ with added CSF components, hence the very flat purple CSF contributions (see Appendix B). Again, it is also clear that no amount of $z = 6$ or 7 star formation can produce the “rising to the red” in all but 4r, with its uncertain star formation at $z = 8$ and noisy SED. Although they look short, these last three epochs add up to half a billion years, or half of the time since the Big Bang, so these are a substantial departure from what seems to be the dominant SFH mode— $\lesssim 100$ Myr starbursts.

The final five examples, 5c, 5r, and row 6, are longer, more continuous histories (SFH4) that stretch over the full redshift range, with four to six epochs of star formation. Although two have a two-epoch gap that could have landed them in the “stochastic” category, for all, there is an orderly history of CSF or declining star formation. These are pronounced examples of young stellar populations with a history of very early star formation that accounts for their strongly “rising-to-the-red” SEDs. All five show $z = 11$ and 12 star formation; however, it is likely that this period of ~ 100 Myr is not “resolved,” so the SED could be reproduced by only one, with the combined mass. Although they represent only 3% of the $z = 6$ population and only 69 galaxies in the 894-galaxy sample (8%), the persistence of SFH4 over the full time range explored here suggests a different environment, one where galaxies can evolve more slowly and relatively undisturbed, for example, experiencing only minor mergers.

From this first set, we see the prevalent signature of early ($z \gtrsim 10$) star formation: an SED rising to the red, often accompanied by substantial star formation at OE. This is best seen by the different levels for the medium bands F335M and F410M, though sometimes only from the broad bands F356W and F444W. This raises the question of whether strong emission lines could be boosting the far red fluxes and mimicking early star formation. We show in Appendix C that this is not the case, the main point being that the CSF templates include active star formation, so that the level of the broad bands cannot be “raised” by emission—it is already included.²⁶ The medium bands F335M and F410M (open circles; not used in the NNLS fit) provide good reference points for the presence of emission and the level in the continuum, because emission-line strengths were not calculated for the narrower bands. Appendix C provides more examples and discussion.

For further examples of SFHs, Figure 3 shows for $z \sim 7$ a virtual replay of the $z \sim 6$ population: five individual bursts (four single, one “twin”); four well-separated “stochastic” events; three more triples; three noisy SFH3/SFH4 histories; three long SFHs, none with a gap of more than one epoch; and two cases with star formation in all six epochs. (Some have large error bars that remind us that these are “representative” SFHs, not to be considered faithful “epoch by epoch.”) As in Figure 2 but not explicitly called out are very high S/N examples; in particular, examples 1l, 2l, 2r, 3r, and 4c are well-defined SED solutions that match the fluxes of the data with remarkable fidelity. Considering the relatively crude redshift resolution of the stellar population templates, the agreement of model and data is convincing evidence that the modeling works and the templates are fully “descriptive”; three or four templates are usually all that is needed, and that is good, because that is all that is available.

Extending the redshift coverage up to $z = 8\text{--}10$ in Figure 4 shows that the classification into the four types of SFHs continues to earlier times. All are represented in similar frequency to those at lower observed redshift. The Lyman break is, of course, pronounced, which helps with constraining the SED_z^* fitting. Most of the the bursts (single and double) in the top three rows rise sharply to the (rest-frame) ultraviolet, signaling very young populations, but conversely, the bottom two rows show the steepest rise to the red in the sample, in this case signaling strongly declining rates of star formation since $z = 12$.

Finally, in Figure 5, we see 18 of the 23 galaxy sample of the highest redshifts. The Lyman breaks are clifflike, and the SEDs are all blue within this sample that covers only 150 Myr, only ~ 200 Myr since $z = 20$ when the first “modern” galaxies were likely born. Rapid evolution of the Universe at this time, especially the strong growth of dark matter halos and rapidly decreasing density of large-scale structure, suggests star formation that might be itself changing in character or composition. Yet, remarkably, the stellar populations we

²⁶ The caveat is emission is much stronger than in the present-epoch star-formation SED_z^* templates: the “rise-to-the-red” could be mistaken for star formation hundreds of Myr earlier. This effect is likely to be seen in the present study, at a level of “factor-of-2-or-less” excess stellar mass for a $< 10\%$ fraction of the SFHs (see Appendix C). For example, SEDs 5l and 5r of Figure 3 are very similar, with strong [O III] emission the only high points, suggesting that the SED rise is due to stronger emission than in the templates. In contrast, the center SED has a steadily rising fit that is certainly the result of the $z = 12$ star formation.

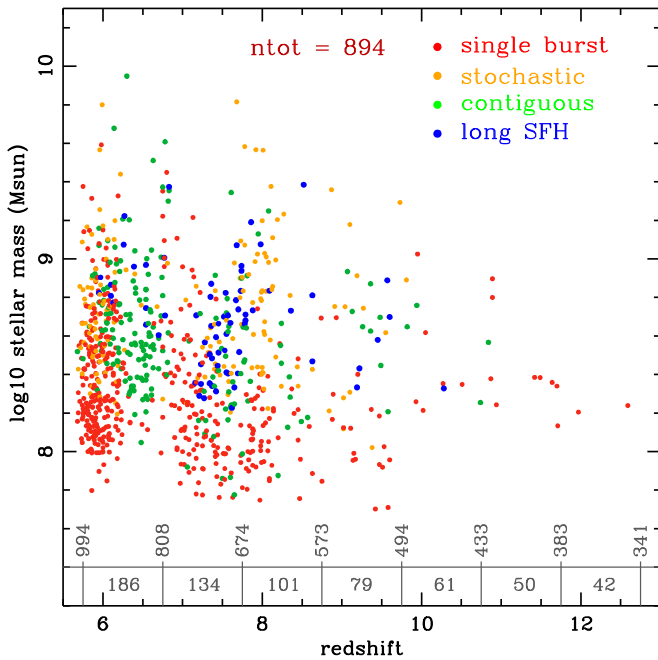


Figure 6. The stellar masses associated with the four SFH types displayed over the full $6 < z < 12$ time frame of this study. The bottom scales are the age of the Universe in megayears and the duration of each of the seven epochs of this study. Each dot represents a galaxy at the OE at its final mass, with SFH type indicated by color. (Figures 8 and 9 show the period spanned by each SFH by “connecting the dots” from the beginning to end of stellar mass growth.) The most important feature in this figure is the presence of all four types over the full range of epochs. Proportions of the four SFH types appear to change over the distribution (for a rough picture, see Figure 7), like the apparent “swells” in long SFHs (SFH4) that appear at $z \sim 7.5$ or contiguous histories (SFH3) at $z \sim 6.5$. These may be the result of a biases in $SEDz^*$ or, for example, large-scale structure, but the full coverage of each SFH type in both epoch and mass is the takeaway.

observe are all matched by the stars that we have all around us today, some 13 billion yr later.

6. SFHs across Time

Does the population of SFHs itself “evolve”? Figure 6 plots the SFH type for 894 different galaxies as measured at their OE, color-coded to show burst SFHs as red and orange (single and multiple) and contiguous “triples” and continuous “long SFHs,” as green and blue. To first order, we see two things: (1) the “final” masses of all 894 galaxies in our SFH sample are largely confined to 10^8 – $10^{10}M_\odot$, and (2) all four types are represented over the full redshift range covered in this study. That there is some “accumulated” stellar mass below 10^8M_\odot but none below $5 \times 10^7M_\odot$ is a simple detection limit: the fluxes would generally fall below the $S/N > 5$ limit we have chosen. On the other hand, the steep falloff in numbers above $M > 3 \times 10^9M_\odot$ is probably a reflection of astrophysics, for example, stellar feedback suppression in the environment of rapid star formation in the compressed volumes of these subkiloparsec-sized sources. Powerful feedback is probably expected in the case of the bursts, but it is less obvious why the longer histories, with lifetimes of hundreds of Myr, would be subject to the same limitations, and yet the distribution here suggests, interestingly, that they are. This, and the clear result that most of the stellar mass in this formative time is made in relatively large starbursts, should place strong constraints on numerical simulations of galaxy growth.

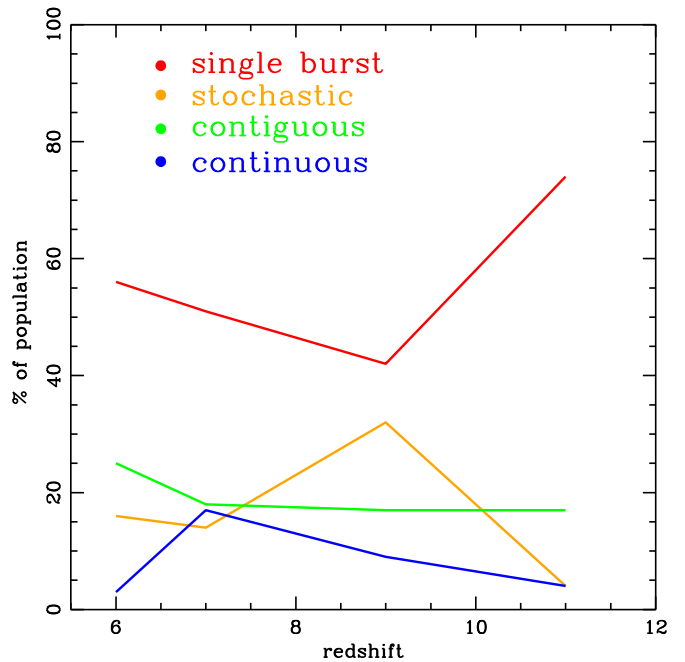


Figure 7. The rough proportions of the four SFH types with redshift, derived from the distribution in Figure 6.

The “evolution” of the proportions of SFHs over time is harder to parameterize, but it is clear from the fact that all types show up over the diagram that there is no strong evolution of the population of SFHs. Figure 7 shows a crude graph of the frequency of the four SFH types for the sample in Figure 6. With the exception of the 70% fraction of bursts at the highest redshifts,²⁷ the variation in the rest of the plot is factors of 2 and not much in the way of trends.

We should add that there is some nonstatistical “bunchiness” in Figure 6, such as the “swells” of SFH3 “contiguous” at $z \sim 6.5$ and SFH4 “long SFHs” at $z \sim 7.5$ and the “valley” of single bursts at $z \approx 6.5$, but we believe that these are more likely $SEDz^*$ “preferences” associated with interpolating between the epochs, rather than a real effect. A denser sampling of epochs, with twice the time resolution for the templates, would likely resolve this, but for now we focus on broad trends.

The lack of strong change over time (for this early period) provides little in the way of clues about the nature or “causes” of the different histories. This suggests that dependencies based on space, rather than time, might provide more insight. We investigate this in Section 8.

7. A Galaxy Is Born

Returning to our theme, we want to explore how the results obtained in this study can help in understanding how galaxies began to grow and build up the essential elements for planets and life. Specifically, how has the progress of star formation proceeded in the first billion years of cosmic history, birthing and growing new galaxies in an environment more gas-rich and more turbulent than we easily imagine? At the same time, these young galaxies are likely fed continuously by a smooth inflow of gas, incorporating less massive galaxies and adding their

²⁷ This probably not a result of small number statistics, as it is the smaller interval of time to express the four SFH types.

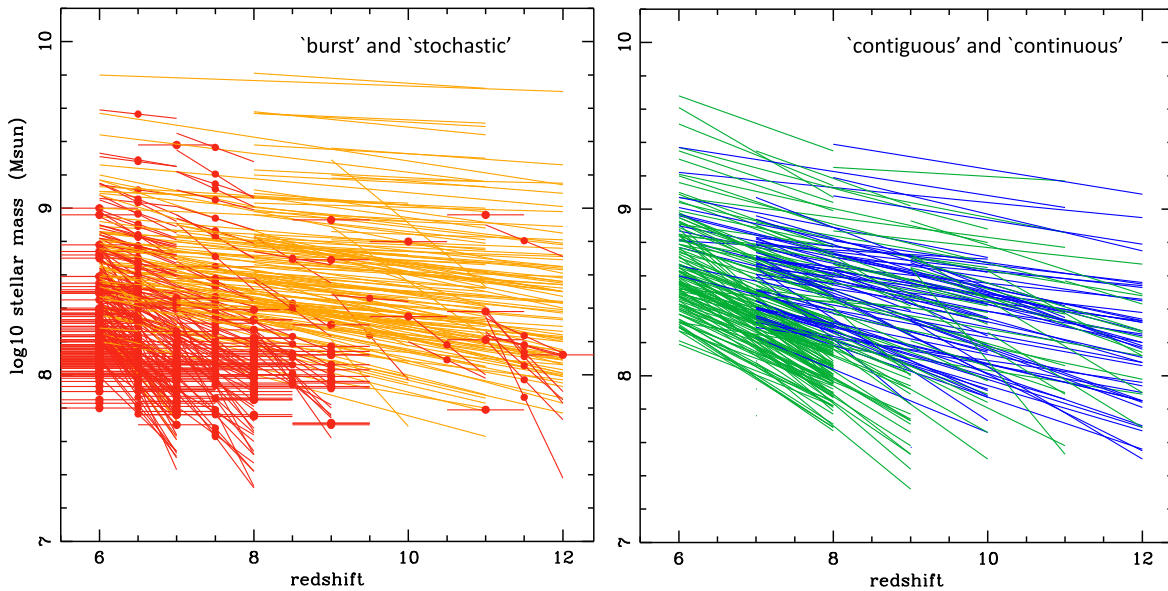


Figure 8. (Left) The contribution to the stellar mass during the period $6 < z < 12$ from galaxies dominated by bursts. Galaxies with SFH1 histories are red dots with “handles” marking their epoch. Orange tracks—SFH2—begin with the first epoch of star formation and connect to the last, showing that such systems do not grow by more than factors of 3 or 4. Instead, new systems appear; that is how total stellar mass grows during this period. The single-burst cases do not add substantial mass until $z \sim 9$ (see Figure 9). (Right) The longer SFHs, both three epochs contiguous (SFH3) and four or more epochs continuous (SFH4), show substantial growth from $z \sim 12$ to 6, reaching a similar level of contributed mass in the range of 10^8 – $10^9 M_\odot$ (Figure 9) but a factor of 3 less than the SFH2 multiple bursts. For both SFH3 and SFH4, the stellar mass accrues over ~ 0.5 – 1.0 Gyr, perhaps suggesting less volatile surroundings and circumstances in their development compared to the SFH1 and SFH2 burst histories.

moderately metal-enriched stellar populations. All this continues as young galaxies are vulnerable to violent major mergers and the huge energy released in massive starbursts and possible large-scale changes through black hole formation and growth. It is not likely that such questions will be answered solely through observations, but rather—as always—theory will be required to explore the physics of each of these elements. Numerical simulations should benefit greatly from these kinds of data, replacing previous and various speculations, where the manifestations of star formation that set the course are reproduced and, we hope, understood.

What we have found in this study already confirms the dynamism of the epoch where galaxies achieved masses of 10^8 – $10^{10} M_\odot$. We find large contributions to the growth of stellar populations by bursts unlike any we see today, strong enough to produce a stellar mass of 10^8 – $10^9 M_\odot$ in an episode lasting only $\lesssim 100$ Myr—little more than a dynamical time—and, apparently, strong enough to ward off further star formation for more than ~ 500 Myr, and maybe even a Gyr. And yet, we also see common cases of multiple bursts over which the total stellar mass can reach well over $10^{10} M_\odot$. What is the difference, then, between these and systems making similar amounts of stellar mass but over the same long period of time where bursting galaxies seem to go dormant?

A good way to appreciate the power of these data can be seen in Figures 8 and 9, where we plot the mass buildup over $6 < z < 12$ from these different modes of star formation. These plots use the SED_z^* SFHs for our 894-galaxy sample to graph the onset of star formation and, in the cases of longer SFHs, its subsequent addition of stellar mass. Here we have “connected the dots”—from when star formation began to the last epoch where it is detected—to show stellar mass buildup. (Color coding is the same as for previous figures.)

Figure 8 shows this for (left) single bursts and bursty “stochastic” histories, SFH1 and SFH2, and (right) longer

“contiguous” and “continuous” histories, SFH3 and SFH4. In an effort to provide guidance to numerical simulation modelers trying to answer such questions, we now express the data we have described here in terms of the growth of galaxies with such different histories in mass-buildup diagrams. The plot is for mass versus time, as in Figure 6, but now with tracks that connect the first and last epochs of recorded star formation within the $6 < z < 12$ era. In Figure 8, SFH1 (a single burst) shows up as a dot, with a handle marking its epoch, while SFH2 (“stochastic”) in orange, appears as a shallow rise, since the two bursts are usually well separated. It is also easy to see that, while the single bursts are the most common SFH type, multiple bursts are both larger in mass to begin with (we find mostly declining SFHs) and growing with subsequent bursts, such that they add the most mass over most of this era. A critical point, though, is that the mass from these burst-dominant galaxies is growing through the appearance of new bursts. The most frequent number of bursts for SFH2 galaxies is just two—a single added burst rather than several. Stellar mass is primarily growing by adding bursting objects, single and multiple, not by many smaller bursts in each galaxy.²⁸ The same diagram for the three epochs “contiguous” (SFH3) and four epochs or more “continuous” (SFH4) histories shows more tilt in its tracks; this is most obvious in the three-epoch tracks that become more and more dominant from redshift $z = 9$ down.

Putting it all together in Figure 9, we combine the burst and longer histories, summing and integrating to learn how the stellar mass of this collection of 894 galaxies grew from $z = 12$ to $z = 6$. We see the contribution of single bursts grow strongly, while the average mass for SFH1—the lowest of the four types—does not increase over the full redshift range. By $z \sim 6$, the single-burst, stochastic, and continuous histories have each

²⁸ Recall that, although we use a burst to represent each epoch of recorded star formation, the stellar mass formed is—from later epochs—unresolved. The “dotlike” representation of SFH in the SED_z^* plots is only symbolic.

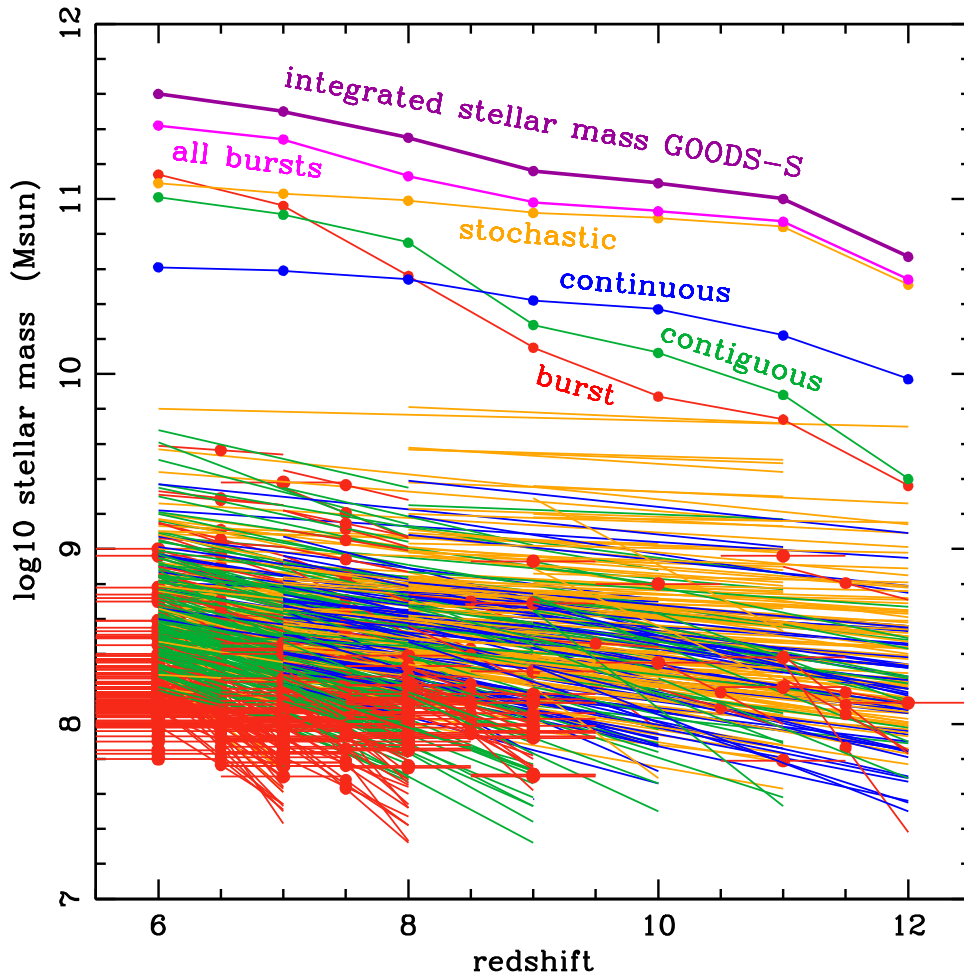


Figure 9. The combined diagram showing all (beginning to end) histories, summed to produce the integrated mass (recorded as the colored lines above). The substantial growth in stellar mass that happens in this volume of space from $z = 12$ to 6 is mostly from adding sources, amounting to the 894 we collected for our study. SFH1 and SFH3 rise rapidly and reach nearly the same value of $\sim 10^{11} M_{\odot}$. SFH2 accumulates as much mass but is flatter because, typically, these begin with an strong early burst and end with a much later smaller one. The contribution of SFH4 is also flatter, rising by only a factor of ~ 3 , due to declining mass contributions in this case. SFH4 histories contribute a factor of 3 less mass than the others, the result of their lower frequency of 8%. Making the principal point of this paper again, SFH1 and SFH2 combine to contribute $2.6 \times 10^{11} M_{\odot}$ of the total stellar mass—66%. Starbursts rule.

added $\sim 10^{11} M_{\odot}$ to this volume of space. The SFH4 galaxies have contributed a factor of 3 less mass, but most of this is the result of their lower frequency of 8%, so this means that all four types contribute a similar amount of stellar mass from $6 < z < 12$. Finally, we plot the integrated stellar mass for this special epoch, which reaches $4 \times 10^{11} M_{\odot}$ in this volume at $z = 6$ and is growing at a rate of $\sim 500 M_{\odot} \text{ Myr}^{-1}$.

We hope that both the rates and manner of star formation in these youngest of galaxies will provide the first meaningful constraints for numerical modeling studies of the evolution of the Universe at the end of the first billion years of cosmic history.

8. SFHs across Space

SFHs are known to have a strong spatial variance, in the sense that different kinds of galaxies (for example, ellipticals as opposed to spirals) are found to dominate in different environments (Dressler 1980), and the different SFHs of these have clearly differed greatly. Recognizing this, we looked at the spatial distributions to see if galaxy “environment” could be connected to the four types of SFHs. Figure 10 shows the distribution on the sky of the four SFHs (again with the same

color coding). There is obvious large-scale structure in the z_1 , z_2 , and z_3 maps, especially in the lowest redshift $z \sim 6$ map, where the contrast between large voids and substantial clustering is strong. This is probably both a result of the growing clustering with epoch and because our much larger sample makes any contrast more discernible. Still, there is a strong impression of substantial large-scale structure over the period $6 < z < 10$ —covering most of the epoch of reionization. A map of only the 23 galaxies in the z_4 sample is not useful, of course, but we have made another view of the $z = 11$ –12 Universe that we discuss below.

It is not surprising that there are no visual spatial distribution differences in the four SFHs, but it is reasonable to expect that correlations of SFH types with local density or nearest-neighbor distance might provide some insight into whether the environments of these galaxies influence their SFHs. In Figure 11 (Appendix A), we show histograms of local density and nearest-neighbor distance for the $z \sim 6$, $z \sim 7$, $z \sim 8$, 9 redshift ranges (a.k.a., z_1 , z_2 , z_3). The left three panels show density ranges that vary from a few to tens of galaxies arcmin^{-2} . As with Figure 6, the most notable feature of these diagrams are ups and downs likely associated with density fluctuations, with no clean separation by type. Perhaps there is

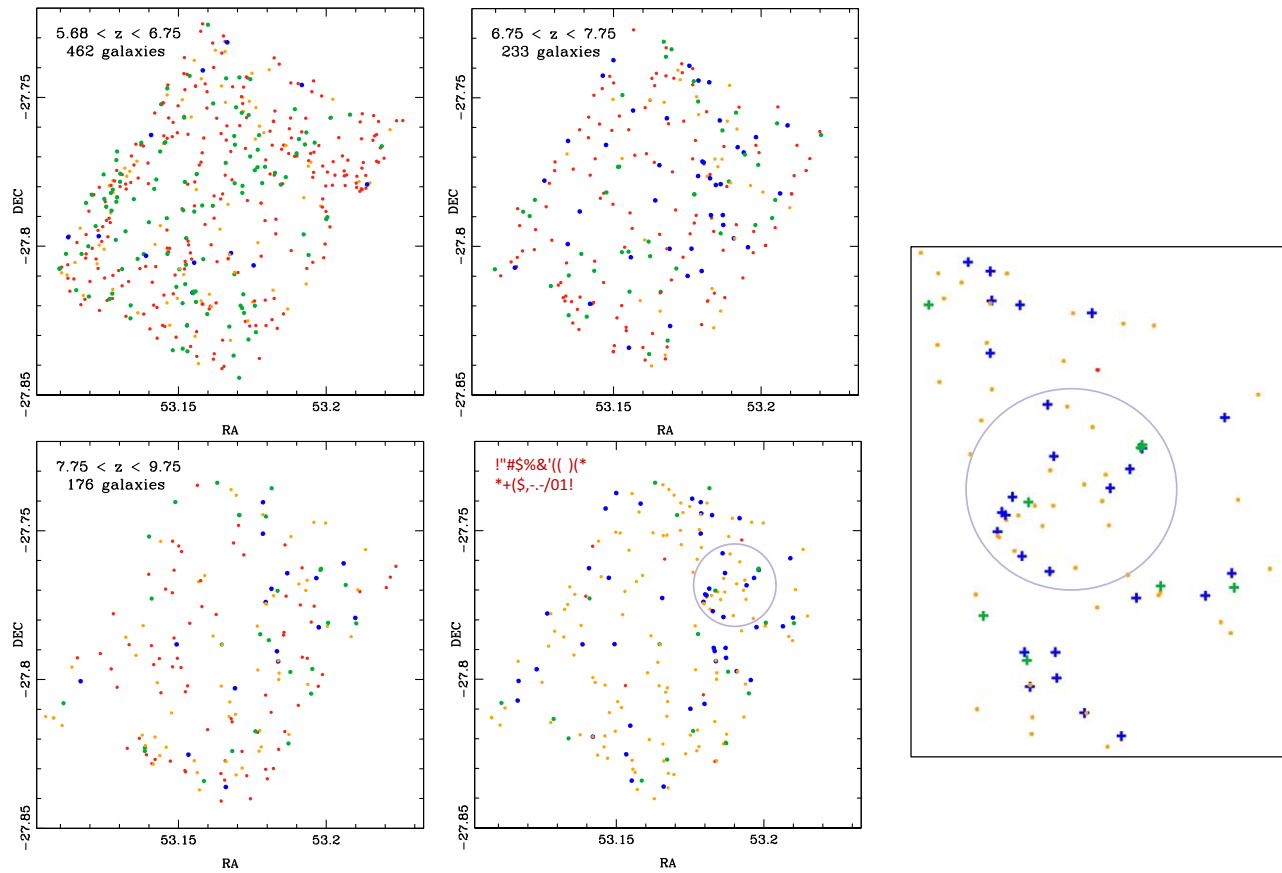


Figure 10. The distribution on sky for the three z_1 , z_2 , z_3 redshift ranges, along with a map of galaxies found by $SEDz^*$ to have had “first star formation” at $z \sim 11$ –12 (lower right; see text). The four boxes on the left essentially cover the full period of reionization. Large-scale structure, in the form of large voids and swaths of higher galaxy density, is evident in each map for the z_1 , z_2 , and z_3 samples. The SFH of each galaxy is represented by color: SFH1, burst = red; SFH2, stochastic (multiburst) = orange; SFH3, three contiguous epochs of star formation = green; and SFH4, long, continuous star formation = blue. However, there are no obvious correlations between location with respect to other galaxies of different SFH types visible from these maps, so if these exist, they must hold for higher-density contrasts. The bottom-right square map shows just such a higher concentration of galaxies—those with “first star formation” at $z = 11$ –12 (this tight group is also visible in the panel above), with the surprisingly clear result that the rarest of our SFHs—long and continuous—are highly represented compared to the study sample. An enlargement of the area ($\sim 2'$) appears on the right.

a slight preference for the longer SFHs to be in denser regions or closer to their neighbors, but nothing clear enough to be helpful.

However, in the sky maps of Figure 10, the fourth panel may hold an important clue about the role of environment. Here we have done something new, based on the ability of $SEDz^*$ to identify prior star formation from galaxies observed at later epochs—galaxy SFHs. We made this map by choosing galaxies for which substantial star formation has been detected at $z = 11$ or 12,²⁹ and in doing so, we selected 201 galaxies of our sample of 894 that had their first epoch of star formation at that time; we plot in the fourth panel what a sky with galaxies forming stars at $z = 11$ –12 might have looked like.

Remarkably, we see a relatively tight galaxy group of 30 members in an area of less than $\sim 2 \text{ arcmin}^{-2}$. Eleven of those, 37%, are SFH4—long, continuous SFHs, only 8% of the full sample in this study. We claim that this detection of many long SFHs “spatially,” while not statistically conclusive, is a unique data point in the search for an environmental dependence of SFH type. Furthermore, this distribution further confirms that $SEDz^*$ actually works; there is no other explanation for how these two quantities—position on the sky and SFH—could be

well correlated. If the $z = 11$ –12 star formation $SEDz^*$ detected were bogus, these galaxies should spread randomly across the field.³⁰ The clustering, as well as what appears to be large-scale structure for the full sample of galaxies, confirms these “earliest” SFHs. In addition, above and below the circled area, the density remains high and appears to contain a higher fraction of SFH4 galaxies, compared to the much larger sample of the left side of the figure.

Subsequently, we noticed that this higher galaxy density region also appears in the upper right panel, $6.75 < z < 7.75$. In fact, this galaxy group had already been independently discovered by members of the JADES team (Endsley et al. 2023) at an observed redshift of $z \sim 7.5$, further confirming their long SFHs. Even more members are observed at the later epoch.

This fortunate “feature” of the GOODS-S field called to mind that, for the original morphology–density relationship, Dressler (1980) and Postman & Geller (1984) found no gradient in morphological type beyond the rich-cluster boundaries, that is, no slowly changing populations beyond the effective radius of the cluster. This and other evidence

²⁹ We consider these epochs to be effectively indistinguishable.

³⁰ Dressler et al. (2018) found a similar spatial dependence for late bloomers and argued that their affinity for other late bloomers confirmed the legitimacy of their unconventional SFHs.

convinced Dressler (see Section IV-C) that the origin of the morphology–density relation did not lie in the late-time evolution of the cluster or its galaxies. Rather, it pointed to an environmental dependence arising at the epoch of galaxy birth: the different morphological types were foretold by their birth environment, a kind of early nurture that is in fact nature.

Soon there will be more deep-field imaging like GOODS-S, and more groups will be found at—incredibly— $z \sim 12$. This result, if confirmed by many other cases, might suggest a rather obvious conclusion about the different SFHs we have found here: burst histories are most common in the equivalent of the lower-density “field” of the modern Universe, probably the result of stochastic merger events that reflect the sparser environment. In this picture, long SHFs are destined for the richer, denser environments of the future. They will be galaxies that, unlike the “bursts,” were built up in a more orderly series of accretion events and minor mergers.

9. Writing Chapter 3: The Age of Starbursts?

Observations of the early Universe with the incomparable JWST have already had a profound effect on our ideas about how the first galaxies were born and how they grew. In scarcely more than a year, hundreds of studies have feasted on galaxy samples that are large, deep, various, and multiplexed. They have been probed with diverse modes of cameras and spectrographs that are unprecedented in a space telescope, offering factors of hundreds to thousands greater sensitivity in the near-to-mid-IR: the early Universe is viewed anew.

Our study is but one of multitudes focused on the rise of stars and galaxies, the elements that redefined the Universe at the very epoch we now explore, for the first time. So far, this wealth of JWST data tells a new story: that the birth of galaxies appears to be a volatile affair. Specifically, a central theme has been that “starbursts” are prevalent in this first billion years, or at the very least, that they play a critical role in understanding what see. Before comparing the present work to a small sample of these papers, it is important to reiterate why—for a majority of galaxies in our GOODS-S field—we identify their SFHs as “bursts.” Our study has particular significance because it was the first to trace the buildup of the stellar mass in the first galaxies (Dressler et al. 2023), and because it is the only one to rely solely on the light of main-sequence A stars. The mass-to-light ratios of these stars are thus accurately known and independent of chemical composition. Furthermore, a stellar population with an age of between 100 and 1000 Myr is not a dusty one; even while O and B stars are still forming in H II regions, A stars have already migrated into near-dustless environments.

Our study of 894 newborn galaxies at $6 < z < 12$ has shown that their star formation was predominately in bursts; we have called these histories “starbursts” (single) and “stochastic” (multiple). Because of the methodology of this study and the limitations of SEDs with seven broadband fluxes, we actually know little about the nature of these bursts that we find dominating the SFHs of the first galaxies. For these, we observe primarily, almost exclusively, the light of A stars whose ages range between ~ 50 and 150 Myr. It is likely that the mass of stars born during the full epoch was much less than that of those born in the first $\lesssim 50$ Myr of explosive star formation that preceded it. In other words, most of the observed A stars came from a shorter period that started early in the epoch. By this reasoning, we suggest that SFRs of $10\text{--}30 M_{\odot} \text{ yr}^{-1}$ characterized

the dust-enshrouded phase we have imagined, and it is during this phase that the $\sim 50\text{--}120$ Myr old A stars that define our SEDs were born. We can estimate the SFRs of the CSF at OE and imagine them to be typical of the SFR over the whole epoch; that might only be $1\text{--}10 M_{\odot} \text{ yr}^{-1}$ (see, for example, Emami et al. 2019; Faisst et al. 2019; Rezaee et al. 2023), but we will be hard-pressed to make an SED measurement, or any other we can think of, that can recover that history of the SFR with a resolution of tens of megayears for any given object.³¹

It is more accurate, then, to say that our study has concluded that starbursts dominate not because we see signatures of $10^8\text{--}10^9 M_{\odot}$ of stars forming over an epoch but because we see a population of A stars in that epoch that are limited to ages of less than $\lesssim 150$ Myr. Most likely, they were born in a much shorter period early in that epoch. What defines our result that “starbursts dominate” is that we see no A stars older than, say, 150 Myr, that is, from a prior epoch. That is why we call these SFHs bursts, not because we are seeing the burst (although we may be, in some cases), but because the only stars we do see are young.

We think that the principal benefit of our observations of the prominent role of starbursts will be to help inform theory and numerical simulation models about the growth of the baryonic component of the Universe that winds up as galaxies. The prevalence of bursts of star formation in the first billion years should be influential in guiding theoretical work to understand galaxy growth in a dynamic environment. It also seems that there are environmental factors that might send galaxies down one path rather than another that could help constrain numerical simulations.

Early results from JWST have focused on a large population of bright galaxies, particularly at $z > 10$, e.g., Donnan et al. (2023), Harikane et al. (2024), and Finkelstein et al. (2023), suggesting that the luminosity function of the first galaxies evolved less slowly with redshift.³² Observations of galaxies that are brighter than expected, more numerous than expected, or evolving less rapidly than expected have promoted “burstiness” as a way to reconcile these findings (e.g., Looser et al. 2023) with previous models (e.g., Wilkins et al. 2022). However, those galaxies are higher redshift and/or rarer (and more massive?) than those studied here, so our sample adds little to that discussion.

On the other hand, Sun et al. (2023a, 2023b) have in particular suggested that lower-mass galaxies, with an abundance and mass predicted with pre-JWST models, have been elevated in luminosity by bursts, specifically that their light-to-mass ratios have risen through substantial bursts of star formation. While again, those samples are not comparable our own, we can by analogy question this explanation. Our study finds a high level of “burstiness” through measurements of stellar mass—the mass of A stars from the SEDs. Likewise, the $z > 10$ “bright” examples may be cases of galaxies forming more stellar mass in bursts.

In a study that also seeks to measure a change in SFHs over $6 < z < 12$, Ciesla et al. (2023) use a very different method than our own to extract such information from SEDs. Their analysis

³¹ Alternatively, spectroscopic measurements of emission-line spectra for these kinds of galaxies could be used in a statistical way to estimate the range of SFRs and the level of “burstiness” for the sample and by comparing SFRs from UV flux to those from H α for large samples.

³² That is, the luminosity function is not declining as rapidly as pre-JWST (HST) observations and derived predictions.

correlates SED shape with position on the star-forming main sequence to characterize whether a galaxy’s SFH is “stochastic,” like our definition—bursty over multiple epochs—or “secular”—longer and steadier, like our SFH3 and SFH4 types. They posit a smooth transition from mostly stochastic to mostly secular at around $z \sim 9$. Although our sample is relatively small beyond $z > 9$, Figure 6 shows no clear transition at $z > 9$, with a similar fraction of SFH1+SFH2 and SFH3+SFH4 down to $z \sim 7$. There seems to be a strong upturn in both SFH1 and SFH3 below $z \sim 7$ (see Figure 7 with the ratio between “stochastic,” SFH1, and “secular,” SFH3, basically unchanged). Again, our methodology is more straightforward— SED_z^* actually derives SFHs from ages of A-star populations, but this important issue requires further study.

About this important matter, what seems clear is that most of the youngest galaxies do not grow steadily in a calm, peaceful environment. Rather, their journey to what we today regard as “galaxy-sized” may be more chaotic, or even explosive. Perhaps these are gas-rich mergers dominating in lower-density regions, manifesting in “one- or two-event” growth spurts in the first billion years, reaching $\sim 10^9 M_\odot$ (what we now call galaxy-sized) when this first phase completes. Importantly, however, by $z \sim 2$ —“cosmic noon”—these galaxies should grow by an order of magnitude in mass to reach a halfway point for L^* . It will be important, and challenging, to relate that later, more easily observed Universe to what we have witnessed for the earliest galaxies. These starburst galaxies at $6 < z < 12$ seem neither poised for another burst nor prepared to settle into steadier SFHs. The simple fact that most of our 894 galaxies do not show star formation over many epochs precludes the notion that these bursty objects are “picking up” again before $z \sim 6$. Perhaps the “contiguous” SFH3 galaxies, common in our $z = 6$ sample, are destined to become those L^* galaxies. We note that almost all show the signatures of continuing star formation at $z = 6$, so perhaps they will grow into the most common galaxies of today, just beginning in earnest their journey to maturity. It is undeniable that a transition from “stochastic” to “secular” (to use Ciesla et al.’s term) did occur, so a focused study on $4 < z < 6$ galaxies, by whatever means their SFHs can be characterized, seems a priority, and imperative for Chapter 3.

Finally, pursuing our suggestion that the starbursts we have observed were the consequence of intense, extreme-density, dust-enshrouded bursts of star formation, we hope an effort can be made to match up this population of growing galaxies to a coeval population of heavily dust-obscured protogalaxies that will come from JWST/MIRI and perhaps ALMA. That our sample seems effectively dust-free strongly suggests that there is a “just-before” phase of tens of millions of years in which explosive star formation ignited in gas-rich protogalaxies, leading directly to the objects we have been studying. Forming stars rapidly in these subkiloparsec volumes is a formidable challenge to our considerable knowledge of how stars form. In particular, the feedback from the supernovae of such starbursts should blow things apart.

We have taken note, with great interest, of work suggesting that such feedback can be suppressed if, at that time, supernovae of mass $M \gtrsim 10 M_\odot$ collapsed directly into black holes. Renzini et al. (2022) have suggested that this extraordinary explanation is nearly “mandatory” to explain the multiple stellar populations observed for many globular

clusters, traditionally thought to be limited to a single generation by supernova-driven feedback. It appears that the same challenge applies toward our understanding of the earliest galaxies. We find first “bursts” of star formation with stellar masses $\gtrsim 10^8 M_\odot$ —a scaled-up version of the largest globular clusters—similarly in need of a physics miracle (see Dekel et al. 2023) to avoid destruction before fulfillment.

Travelers on JWST, the ultimate spacetime ship, we seek answers to questions first asked a century ago. Wonderfully, we are fortunate to be grasping this “once-in-a-species” opportunity to know our origins.

Acknowledgments

A.D. gratefully acknowledges the support of the NIRCcam team for the opportunity to contribute to the NIRCcam science program on the earliest galaxies and for prior funding from JWST/NIRCcam contract NAS5-02015. The DC2 “deep-field” simulation was a Herculean task that provided the essential guidance for the program described here and for the NIRCcam GTO program in general.

This work is based on observations made with the NASA/ESA/CSA James Webb Space Telescope, using imaging data processed by the NIRCcam project team in collaboration with JADES, a extragalactic project team consisting of members of the NIRCcam and NIRSspec teams. D.S., K.M., M.R., and A.D. have been supported by JWST/NIRCcam contract to the University of Arizona NAS5-02015.

N.B. acknowledges support from the Cosmic Dawn Center (DAWN), funded by the Danish National Research Foundation under grant No. 140. K.B. acknowledges partial support by the Australian Research Council Centre of Excellence for All Sky Astrophysics in 3 Dimensions (ASTRO 3D) through project No. CE170100013. A.B. acknowledges funding from the “FirstGalaxies” Advanced Grant from the European Research Council (ERC) under the European Union’s Horizon 2020 research and innovation program (grant agreement No. 789056). S.C. acknowledges support by European Union HE ERC starting grant No. 101040227—WINGS. D.E. is supported as a Simons Investigator and by (JWST/NIRCcam) contract to the University of Arizona NAS5-02015. R.H. acknowledges funding for this research from the Johns Hopkins University, Institute for Data Intensive Engineering and Science (IDIES).

We use data from the JADES High Level Science Product at MAST (Rieke et al. 2023).

Appendix A SFHs versus Environment at $z > 6$

The histograms of Figure 11 show distributions of the four SFH types with local density calculated using the area of the 10 nearest-neighbor galaxies and distance to the single nearest-neighbor galaxy. The absence of any obvious trends between SFH type and environment seems at odds with results for environmental dependencies later in cosmic history, for example, the obviously difference in the SFHs of rapidly growing elliptical galaxies compared to the drawn-out SFHs of spirals like the Milky Way. However, from another perspective, the lack of environmental dependence is reminiscent of studies of the environment around rich clusters in the early 1980s (Dressler 1980; Postman & Geller 1984) that found that a steep dependence of galaxy morphology with

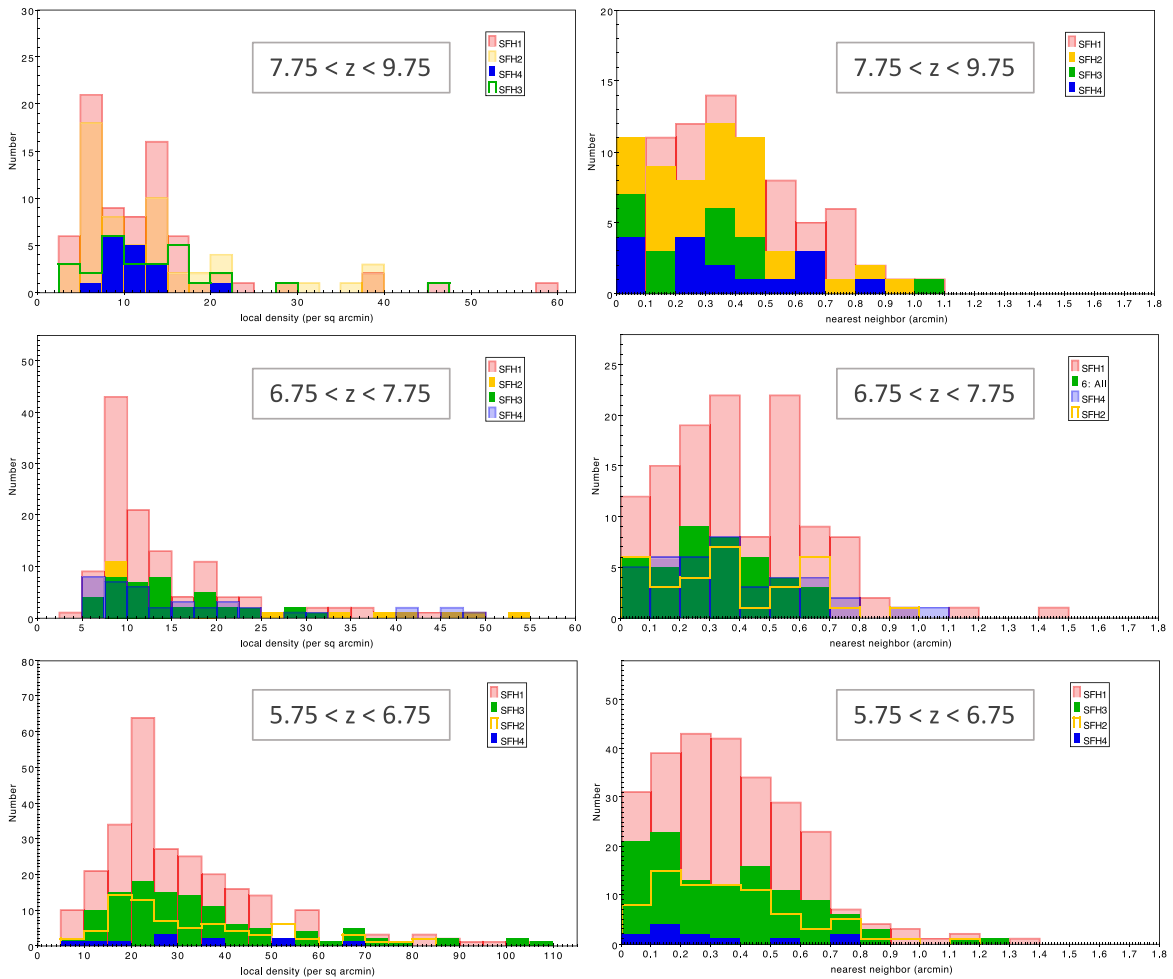


Figure 11. Histograms of the incidence of the different SFH types with local density (left) and as a function of nearest-neighbor separation (right). No clear trends are apparent; that is, SFH types at this early time do not depend on the local environment as they do after $z \sim 2$. The panels from bottom to top are for the three redshift ranges, $z \approx 6, 7,$ and $8, 9$ (z_1, z_2, z_3). The chief differences are in terms of scale; for example, the peak of both distributions shifts to lower density and larger separation with increasing redshift, as expected for a sample limited by apparent brightness. Density contrasts in this GOODS-S field are modest, but Figure 10 shows signs of a correlation of longer SFHs with higher-density groups.

local density within the effective radius of a cluster did not continue to the lower-density “field” beyond. In this study, Figure 10 shows a hint of the same behavior; in the region of higher density, a $z \sim 7$ rich group, the long-SFH types, are strongly represented, a correlation that is not expressed in lower-density surroundings.

Appendix B Stellar Population Templates of SED_z^*

In this section, we show samples of the stellar population templates used by SED_z^* to characterize the SFHs of $5 < z < 12$ galaxies. Figure 12 plots the fluxes of 10 stellar population templates with a 10 Myr burst of star formation (at $1 M_\odot \text{ yr}^{-1} = 10^7 M_\odot$) at the start of epoch $z = 12$, “observed” to evolve at epochs $z = 11 \dots 3$ —later epochs without further star formation. For this study, SED_z^* uses seven templates, for bursts starting at $z = 11, 10 \dots 6$. The principal feature of this plot is that the templates are largely nonconformal, that is, not a conformal set of curves scaled by some parameter or set of parameters. These “vectors” describing stellar populations are different enough—sufficiently orthonormal—that a least-squares combination of them is substantially “resolved” from any other combination. This property allows SED_z^* to

“calculate” the history of a stellar population, essentially, by vector algebra: finding the coefficients of the vector sum that best represent the observed SED.³³ What makes this particular application of the method potent is the nonconformal character of SEDs for stellar populations of ages $\tau < 1$ Gyr—the templates covering the early Universe for $z = 12$ to $z = 5$ whose light is dominated by main-sequence A stars. The figure shows why, as has been known for half a century, only finding the ages of stellar populations with stars older than 2 Gyr is, in practice, impossible; note how the templates $z = 5, 4,$ and 3 are becoming a simple scaling of a single shape, as the Universe reaches an age of 2 Gyr at $z \sim 3$.

The signature of a burst of star formation is a very blue SED at that epoch, but for the subsequent epochs, the history of star formation within that epoch is unresolved. Therefore, SED_z^* accumulates the sum of bursts as the stellar masses of each; this

³³ Another way of thinking about these templates is to consider them as musical “chords,” all playing the same seven “notes” (the wavelengths of the seven wide bands) but differing in the volume (flux) from templates to template. Since all notes sound together, there are limited combinations available to fit the SED (the music), and there is no way to make changes in individual bands to improve the sound (fit). This is why the good SED fits found in this study—with the restricted number of A star-dominated templates from present-day populations—provide a “self-verification” of the method.

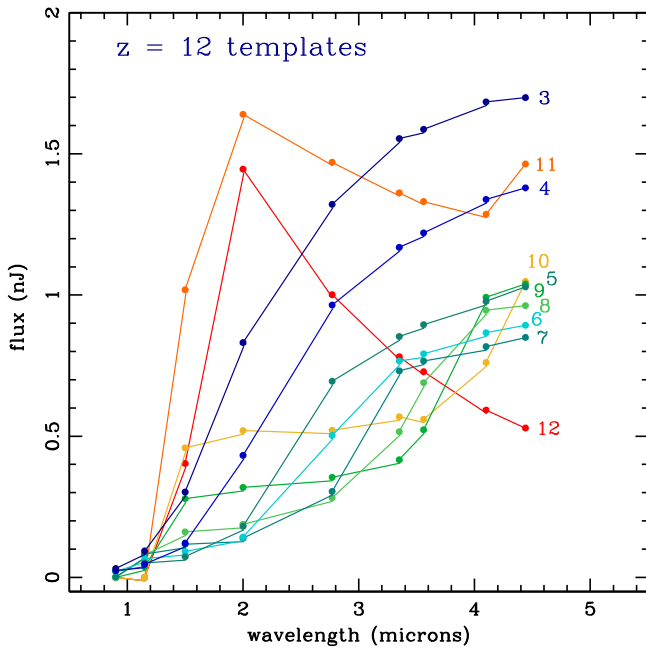


Figure 12. Templates for a 10 Myr burst of star formation at $z = 12$ evolved (aged and observed) at lower redshifts. With good data ($S/N \gtrsim 7$), the distinctive shapes of these templates allow SED_z^* to make essentially unique SFH solutions. This character changes for $z \leq 5$ as the templates become scaled versions of each other, the reason that stellar populations with $\tau > 2$ Gyr are basically indistinguishable, a behavior attributable to the very similar giant branches of older stars.

is indistinguishable from continuous star formation over the prior epochs.

A final point of note is that SED_z^* works because it is strongly constrained by the shape of each template, which means that

variation of the coefficients in the maximum-likelihood solution cannot either make or break the fit. If these templates, made from present-epoch stars in our Galaxy, were not representative of stellar populations at $z > 5$, this attempt to reproduce observed SEDs would fail badly. Quite the opposite is true.

The top-right panel of Figure 13 shows templates for six templates, from $z = 10$ to $z = 5$, corresponding to the flux resulting from $1.0 M_\odot \text{ yr}^{-1}$ of CSF over that particular epoch. Unlike bursts, there is no evolution of stellar population over subsequent epochs, because ongoing star formation can only be recorded in the SED from the OE. Prior epochs of CSF are indistinguishable from bursts of the same mass. With the time resolution offered by broadband SEDs, no additional information is available; there is no signature to distinguish CSF from a more complex behavior over the ~ 100 Myr duration of each epoch.

Clearly, the distinguishing feature of the six CSF templates is that they are all flat—as conformal as it gets—in comparison to the burst templates. The modulation that is apparent comes from the Balmer break—moving from $\sim 2 \mu\text{m}$ at $z \sim 6$ to $\sim 3.5 \mu\text{m}$ at $z \sim 10$, and from the jaggedness of the SED from 3 to $5 \mu\text{m}$ —due to [O III] and $H\alpha$ emission lines. This flatness, when combined with bursts of previous epochs, is responsible for much of the “character” of the long SFHs. The right plot of Figure 13 shows that combining a burst early in an epoch with CSF at that same epoch produces signatures that are found in many $z > 5$ SEDs. The ratios of 3:1 to 1:2 for the burst/CSF flux, shown in this case for $z \sim 7$, are apparent in hundreds of the SEDs in our sample. It is worth remembering that this combination is just equivalent to ongoing star formation that is declining, rather than constant, over the epoch.

The bottom plot shows the attenuation in the SED expected for different values of A_V , as described in Section 2.

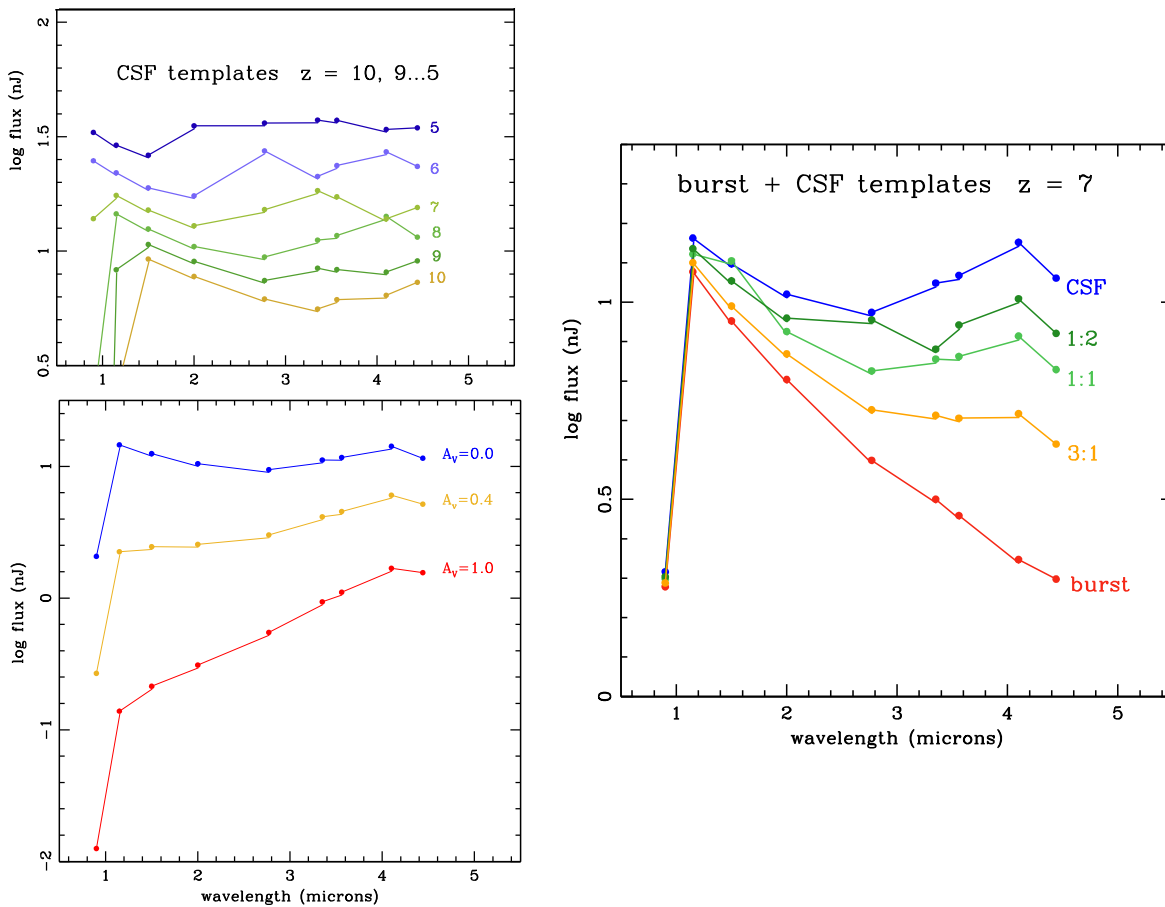


Figure 13. Top left: templates for CSF at epochs 5–10. Right: combinations of burst and CSF templates at $z = 7$. Ratios are CSF to burst (see text). Bottom left: the effect of dust on the $z = 7$ CSF template shown for $A_V = 0.4$, a factor of 2 in the $1.15 \mu\text{m}$ band, and $A_V = 1.0$, a factor of 10, demonstrating that the galaxies in the sample of 894 analyzed here show little if any dust. Even a 30% decline across the SED from 4.44 to $1.15 \mu\text{m}$ —equivalent to $A_V \sim 0.1$ —would have adversely impacted the $SEDz^*$ fit compared to the no-dust solution.

Appendix C

Do Emission Lines Impact Derivations of SFH with $SEDz^*$?

In general, the influence of emission lines in photometric studies using broad bands, like this one, are only significant if the line-to-continuum ratio is very large. For example, a moderate-resolution spectrograph (with resolutions of hundreds) is effective at detecting even weak lines only when the continuum level is low, and that is true only for young stellar populations, $\tau \leq 20$ Myr. In contrast, broad photometric bands like the ones used in this study select against such populations, because the continuum flux is weak (the objects are faint).

Because our detections of faint galaxies rely on the sensitivity to small fluxes, the equivalent width of an emission line must be enormous, that is, a low continuum flux. Since the “integer epochs” of this study cover ~ 100 Myr of cosmic history, any object selected through broadband photometry will by necessity require a large burst of star formation compared to the stellar mass generated over the epoch. Thus, the contribution to the flux of the youngest populations, through emission lines, should be modest.

Figure 14 verifies that by selecting cases of relatively strong star emission lines (the right-side examples) and comparing to SEDs on the left with little evidence of star formation. Our SEDs are made up of seven broad bands (filled circles) and the two medium bands, F335M and F410M (open circles; not used

in the $SEDz^*$ fitting). In particular, these and the F356W and F444W broad bands are sampling the [O III] and $H\alpha$ lines over the redshift range $6 < z < 9$.

The medium bands often provide good evidence of emission because their width is $\sim 40\%$ of the broad bands, so they can also—in cases that exhibit emission—establish the continuum level at that color, sometimes considerably below that of the broad bands.³⁴ The close agreement in flux of both broad and narrow bands in the top and bottom left examples shows that there is little or no detected emission in these cases, which is common in our 894-galaxy sample. Note how the levels of F356W and F444W are close. The middle left SED shows moderate emission in F444W and detection of the continuum in F335M, and here F444W appears to be elevated above F356W by [O III] emission. The case in the top right is a stronger example: strong detected emission in F356W and F335W, also from [O III], at this lower redshift.

When compared to the flat blue (CSF) templates on the left and purple on the right (excluding middle right), these SEDs all show a substantial rise in flux over the F356–F444 region. What is the contribution of emission lines to this rise?

For most of our sample, the answer is little to none. This is because the CSF templates include the emission-line fluxes for

³⁴ It is significant, though, that none of our SEDs show a continuum detection near zero, as would be the case for a pure emission-line spectrum, consistent with our claim that this is not possible with broad bands and long epochs.

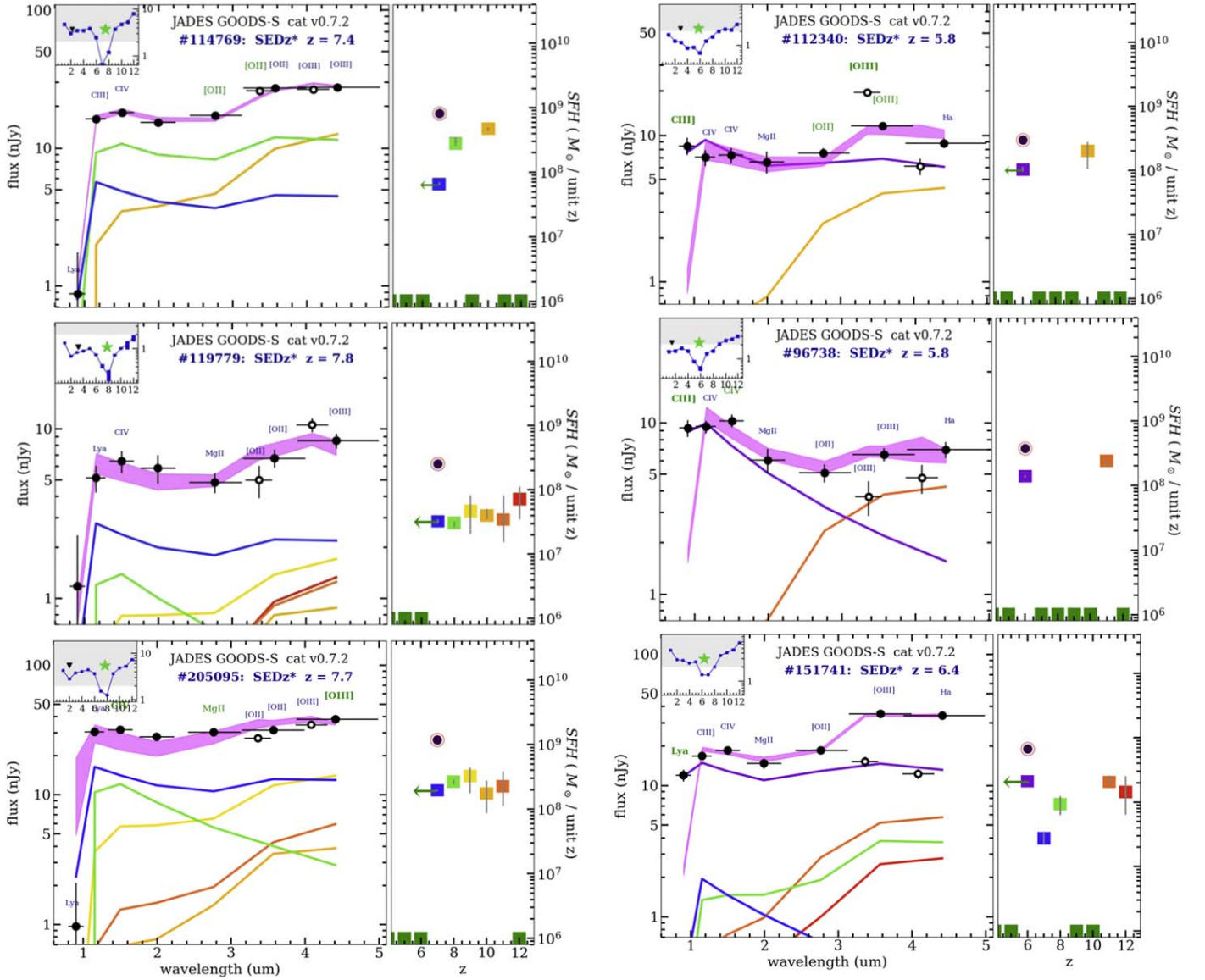


Figure 14. These $SEDz^*$ plots address the influence of emission lines on SFHs derived in this study. The SFHs at top and bottom left have little or no emission, as shown by the fact that the medium bands (2.5 times smaller bandwidth than broad bands) share the same flux level as the broad bands. The middle left shows a modest level of emission—elevation of F410M over F444W—and the top right shows evidence for moderate emission. The fact that the stellar population templates include emission-line flux representative of typical star-forming regions is obvious from the middle and bottom right examples, demonstrating that the “rise of the red continuum” in these six cases must be due to flux from older stellar populations, unless significant contributions from [O III] and/or $H\alpha$ were substantially stronger than those of present-day star formation regions.

the appropriate stellar population for both the broad and narrow bands. As explained in Stark et al. (2013), the SEDs of these templates include hydrogen lines (Robertson et al. 2010; based on Osterbrock tabulations and case B recombination), metallic lines ($Z = 0.2 Z_{\odot}$, likely appropriate for our high- z galaxies), and continuum radiation, calculated and described by Stark et al. (2013). Of course, the strength of these lines should vary from object to object, and perhaps systematically from $z \sim 0$ to $z > 5$, but examination of dozens of our sample suggests that such variations, though present, are smaller than the effect of “line versus no-line.” However, the existence of variation, as well as not knowing the redshift well enough to place the emission lines accurately, prevents us from making detailed arguments about whether these low- z line ratios are in fact a good match for very young galaxies.










Knowing that the emission lines are appropriately included in the templates we use, is it easier to understand the examples we show here. Since emission is included, the F356W and F444W fluxes of the top and bottom left SEDs show no emission; indeed, if their “elevation” from a flat SED were due to emission, the narrow bands would show higher, not at the same level. The middle left example does show elevation of F444W compared to its more typical closeness to the level of F356W, but the $SEDz^*$ model passes through both points because emission is included (this also indicates that the present-epoch templates are appropriate). The same goes for the top right example with strong emission in F335M. In this case, and most others, the continuum level of F410M, compared to the elevated value of F356W, comes in at the proper ratio of 2.5:1.

In the middle and bottom right examples, we again see the SED_z^* model passing through F356W and F444W, and the emission—here [O III] and $H\alpha$ —is included. The continuum below is sampled in each by both medium bands. Here we also see that the continuum level is provided by a single, older, $z = 11$ population, which is boosting the level of F356W and F444 to give the SED its distinctive shape, one that is inconsistent with any single population. For the bottom right example, the continuum is matched by $z = 11-12$ and $z = 8$ flux to complete the fit. The only way emission could contribute significantly would be if [O III] and $H\alpha$ emission were substantially stronger in these regions of star formation in $z > 5$ galaxies than in the galaxies of today.

To look for galaxies with stronger-than-present-day emission, we examined SEDs to find cases where the points indicating emission had fluxes systematically higher than the values of the five bands F090W, F115W, F150W, F200W, and F277W. There were few among the 690 cases of the z1 and z2 samples, $z < 7.75$, but 50 of the 128 galaxies in the redshift range $7.75 < z < 9.75$ showed conspicuous [O III] emission in the F444 band. Among these, 28 had SEDs that rose steadily through F356W, which SED_z^* attributed to earlier star formation, $z \geq 10$. For the remaining 22 the lack of such a clear trend suggested that these were, in fact, cases of [O III] emission much stronger than represented by the templates. For such cases the “earlier” stellar mass found by SED_z^* was incorrect. By examining the $z \geq 10$ contribution, we determined that for such galaxies total stellar mass had been overestimated by factors of 1.5 to 3.5. This is important for future SED_z studies. At the same time, it does not alter the conclusions of this study, in fact, it moves some SFH2 types (an early and late burst) back to the SFH1 category, reaffirming our principal result of the prominence of starbursts in the early universe.

Since these strong emission cases are a small part of the study, this result, added to the cases with little or no emission, confirms that “red rise” we find for ~ 100 galaxies is flux from older stellar populations, in other words, SED_z^* star formation histories confirmed.

ORCID iDs

Alan Dressler  <https://orcid.org/0000-0002-6317-0037>
 Marcia Rieke  <https://orcid.org/0000-0002-7893-6170>
 Daniel Eisenstein  <https://orcid.org/0000-0002-2929-3121>
 Daniel P. Stark  <https://orcid.org/0000-0001-6106-5172>
 Chris Burns  <https://orcid.org/0000-0003-4625-6629>
 Rachana Bhatawdekar  <https://orcid.org/0000-0003-0883-2226>
 Nina Bonaventura  <https://orcid.org/0000-0001-8470-7094>
 Kristan Boyett  <https://orcid.org/0000-0003-4109-304X>
 Andrew J. Bunker  <https://orcid.org/0000-0002-8651-9879>

Stefano Carniani  <https://orcid.org/0000-0002-6719-380X>
 Stephane Charlot  <https://orcid.org/0000-0003-3458-2275>
 Ryan Hausen  <https://orcid.org/0000-0002-8543-761X>
 Sandro Tacchella  <https://orcid.org/0000-0002-8224-4505>
 Christopher Willmer  <https://orcid.org/0000-0001-9262-9997>

References

- Bruzual, G., & Charlot, S. 2003, *MNRAS*, **344**, 1000
 Ciesla, L., Elbaz, D., Ilbert, O., et al. 2023, *A&A*, submitted (arXiv:2309.15720)
 Couch, W. J., & Sharples, R. M. 1987, *MNRAS*, **229**, 423
 Curtis-Lake, E., Carniani, S., Cameron, A., et al. 2023, *NatAs*, **7**, 622
 Dekel, A., Sarkar, K. C., Birboim, Y., Mandelker, N., & Li, Z. 2023, *MNRAS*, **523**, 3201
 Donnan, C. T., McLeod, D. J., McLure, R. J., et al. 2023, *MNRAS*, **520**, 4554
 Dressler, A. 1980, *ApJ*, **236**, 351
 Dressler, A., Brown, R. A., Davidsen, A. F., et al. 1996, Exploration on the Search for Origins: A Vision for Ultraviolet-Optical-Infrared Space Astronomy, NASA STI/Recon NASA-TM-112149, NTRS - NASA
 Dressler, A., & Gunn, J. E. 1983, *ApJ*, **270**, 7
 Dressler, A., Kelson, D. D., & Abramson, L. E. 2018, *ApJ*, **869**, 152
 Dressler, A., Vulcani, B., Treu, T., et al. 2023, *ApJL*, **947**, L27
 Eisenstein, D. J., Willott, C., Alberts, S., et al. 2023, *ApJS*, submitted (arXiv:2306.02465)
 Emami, N., Siana, B., Weisz, D. R., et al. 2019, *ApJ*, **881**, 71
 Endsley, R., Stark, D. P., Whitley, L., et al. 2023, *MNRAS*, **524**, 2312
 Faisst, A. L., Capak, P. L., Emami, N., Tacchella, S., & Larson, K. L. 2019, *ApJ*, **884**, 133
 Finkelstein, S. L., Bagley, M. B., Ferguson, H. C., et al. 2023, *ApJL*, **946**, L13
 Hainline, K. N., Hviding, R. E., Rieke, M., et al. 2020, *ApJ*, **892**, 125
 Harikane, Y., Nakajima, K., Ouchi, M., et al. 2024, *ApJ*, **960**, 56
 Kelson, D. D., Benson, A. J., & Abramson, L. E. 2016, arXiv:1610.06566
 Kelson, D. D., Williams, R. J., Dressler, A., et al. 2014, *ApJ*, **783**, 110
 Lawson, C., & Hanson, R. 1995, *Solving Least Squares Problems* (Philadelphia, PA: SIAM)
 Looser, T. J., D’Eugenio, F., Maiolino, R., et al. 2023, arXiv:2306.02470
 Merlin, E., Bonchi, A., Paris, D., et al. 2022, *ApJL*, **938**, L14
 Morgan, W. W., & Keenan, P. C. 1973, *ARA&A*, **11**, 29
 Nanayakkara, T., Glazebrook, K., Jacobs, C., et al. 2023, *ApJL*, **947**, L26
 Postman, M., & Geller, M. 1984, *ApJ*, **281**, 95
 Renzini, A., Marino, A. F., & Milone, A. P. 2022, *MNRAS*, **513**, 2111
 Rezaee, S., Reddy, N. A., Topping, M. W., et al. 2023, *MNRAS*, **526**, 1512
 Rieke, M., Robertson, B., Tacchella, S., et al. 2023, Data from the JWST Advanced Deep Extragalactic Survey (JADES), STScI/MAST, doi:10.17909/8TDJ-8N28
 Rieke, M. J., Kelly, D. M., Misselt, K., et al. 2023, *PASP*, **135**, 028001
 Rieke, M. J., Robertson, B. E., Tacchella, S., et al. 2023, *ApJS*, **296**, 16
 Robertson, B. E., Ellis, R. S., Dunlop, J. S., McLure, R. J., & Stark, D. P. 2010, *Natur*, **468**, 49
 Robertson, B. E., Tacchella, S., Johnson, B. D., et al. 2023, *NatAs*, **7**, 611
 Stark, D. P., Schenker, M. A., Ellis, R., et al. 2013, *ApJ*, **763**, 129
 Sun, G., Faucher-Giguère, C.-A., Hayward, C. C., et al. 2023b, *ApJL*, **955**, L35
 Sun, G., Faucher-Giguère, C.-A., Hayward, C. C., & Shen, X. 2023a, *MNRAS*, **526**, 2665
 Tacchella, S., Eisenstein, D. J., Hainline, K., et al. 2023, *ApJ*, **952**, 74
 Treu, T., Roberts-Borsani, G., Bradac, M., et al. 2022, *ApJ*, **935**, 110
 Wilkins, S. M., Vijayan, A. P., Lovell, C. C., et al. 2022, *MNRAS*, **519**, 3118
 Williams, C. C., Curtis-Lake, E., Hainline, K. N., et al. 2018, *ApJS*, **236**, 33